Evolution of the grass leaf by primordium extension and petiole-lamina remodeling

A. E. Richardson[1,2,3†*], J. Cheng[1,4,5], R. Johnston[6,7], R. Kennaway[1], Brianne R. Conlon[6], A.B. Rebocho[1], H. Kong[4,5], M. J. Scanlon[6*], S. Hake[2], E. Coen[1*]

[1] John Innes Centre, Norwich Research Park, Colney Lane, Norwich, NR4 7UH.

[2] ARS/USDA Plant Gene Expression Center, 800 Buchanan Street, Albany, 94710.

[3†] Institute of Molecular Plant Science, School of Biological Sciences, University of Edinburgh, Kings Buildings, Max Bourne Crescent, Edinburgh, EH9 3BF.

[4] State Key Laboratory of Systematic and Evolutionary Botany, CAS Center for Excellence in Molecular Plant Sciences, Institute of Botany, Chinese Academy of Sciences, Beijing 100093, China.

[5]College of Life Sciences, University of Chinese Academy of Sciences, Beijing 100049, China.

[6] Plant Biology Section, School of Integrative Plant Science, Cornell University, Ithaca, NY14853.

[7] The Elshire Group Limited, Palmerston North 4472, New Zealand.

[†]Current address

*Corresponding Authors: annis.richardson@ed.ac.uk, mjs298@cornell.edu, enrico.coen@jic.ac.uk

One sentence summary

Developmental genetics and computational modelling unravel the mystery of how the grass leaf develops.

Abstract

The sheathing leaf found in grasses and other monocots is an evolutionary innovation, yet its origin has been a subject of longstanding debate. Here we revisit the problem in the light of developmental genetics and computational modelling. We show that the sheathing leaf likely arose through *WOX*-gene-dependent extension of a primordial zone straddling concentric domains around the shoot apex. Patterned growth within this zone, oriented by two polarity fields, accounts for wild-type, mutant and mosaic grass leaf development, whereas zone contraction and growth remodelling accounts for eudicot leaf development. In contrast to the prevailing view, our results suggest that the sheath derives from petiole, whereas the blade derives from the rest of the eudicot leaf, consistent with homologies proposed in the 19th century.

Main Text

The grass leaf is a conundrum. Unlike a eudicot leaf, which typically has a broad lamina, narrow petiole and basal stipules (Fig.1A-C), the grass leaf has a cylindrical sheath supporting a strap-like blade (Fig.1D-F). The encircling sheath, a derived feature of monocots (*1*, *2*), allows grasses to grow in height during the vegetative phase without extending stem internodes, keeping the apical meristem protected close to the ground.

Evolution of the sheathing leaf presents two problems. First, unlike eudicot leaf primordia, which derive from a fraction of the apical meristem circumference, sheathing leaves derive from founder cells that encircle the meristem(*1*, *3*, *4*) (Fig.1G-J). It is unclear how genes control this extension and subsequent primordium shaping.

Second, the origins of sheath and blade are uncertain. In the 19th century, sheath was considered homologous to petiole, and blade to lamina: the *petiole-sheath* hypothesis (Fig.1K)(*5*). By the 20th century, the petiole-like parallel venation of grasses led to the idea that the entire grass leaf derives from the petiole (phyllode theory, (*6*–*9*), Fig.1L). Further comparative developmental studies led to the current *petiole-leaf* hypothesis: the grass leaf largely derives from the petiole base, while the tip (forerunner tip, or Vorläuferspitze) derives from the upper petiole and lamina (*1*, *10*–*14*) (Fig.1M). Here we revisit these problems through a combination of developmental genetics and computational modelling.

The grass leaf primordium emerges from a primordium zone (PZ, white dotted outline, Fig.1N), which lacks *KNOX* expression(*15*). The PZ straddles concentric domains that will give rise to the adaxial (upper) and abaxial (lower) regions of the leaf (blue, orange). These domains meet at a midplane boundary (green) (*16*, *17*). The PZ is subdivided mediolaterally (Fig.1O,P) into central (blue), lateral (red) and marginal (cyan) domains(*18*). Marginal identity depends on *NARROWSHEATH* genes (*NS1* and *NS2*), members of the *WUSCHEL-RELATED HOMEOBOX* (*WOX*) gene family (*19*, *20*). *ns1/2* double mutant leaf primordia do not fully encircle the apex, and produce leaves with narrower sheaths and proximal blades (*21*).

To understand how these domains control leaf morphogenesis, and to clarify the homology hypotheses' predictions, we modelled their growth. In simulations,

morphology is an emergent property that depends on how specified local growth rates interact with mechanical tissue constraints.

To simulate primordium emergence, we built on a recently proposed model based on growth oriented by two orthogonal polarity fields(*22*). The first polarity field (orthoplanar) runs from the outer tissue surface towards the ad-abaxial midplane (green, Fig.2A-B) to orient growth for primordium emergence, and towards an axial domain (dark blue, Fig.2B) to orient apex growth. Growth rates are specified in two orientations: K_{OP}, parallel to the orthoplanar polarity, and K_{PER}, perpendicular to orthoplanar polarity. Setting K_{PER} greater than K_{OP} in the PZ and apex, generates a ring-shaped primordium encircling the apex(Fig.2C-D).

To generate a sloping primordium, we modulated K_{PER} with the mediolateral identities(Fig.2E-F). However, the primordium lacks an upwardly-growing tip, unlike the real grass leaf primordium (Fig.2F cf Fig.1H), suggesting that a second polarity field, running parallel rather than orthogonal to the tissue surface, may be required to shape the primordium.

To determine the orientation of this second polarity field we analysed an early indicator of epidermal polarity in grasses: the auxin transporter SISTER-OF-PINFORMED1 (SoPIN1)(*23*). Whole-mount immunolocalization of SoPIN1 in barley (*24*) revealed epidermal polarity converging at the primordium midpoint (green signal, white arrows, Fig.2G-H). We therefore introduced a proximodistal polarity field (blue arrows, Fig.2I), pointing from the PZ boundary towards the midpoint. Local growth rates could then be specified in three orientations: parallel to orthoplanar polarity (K_{OP}), parallel to proximodistal polarity (K_{PD}), and perpendicular to both (K_{PER})(Fig.2I). Low K_{OP} and combined mediolateral and proximodistal modulation (Fig.S2G-H) of K_{PD} and

97 K_{PER} generated a sloping ring primordium with a shape and polarity pattern resembling
98 that observed experimentally (Fig.2I-K cf. Fig.1G, Fig.2L cf. Fig.1H).
99 To test whether this model could account for the *narrowsheath1/2* (*ns1/2*)
100 mutant, we first determined PZ extent in wild type and mutant using the *CUP-*
101 *SHAPED-COTYLEDON2* (*CUC2*) boundary gene (*25*). In wild type, *CUC2* expression
102 encircled the meristem, whereas in *ns1/2,* the PZ was truncated by a new *CUC2*
103 expression boundary (Fig.2M-N). To model the *ns1/2* mutant, we similarly truncated
104 the PZ by removing the marginal domain (Fig.2O). This removal generated a narrower
105 primordium (Fig.2P-Q) that matched the morphology of *ns1/2* (*20*).
106 We next studied formation of sheath and blade. The marginal regions of the
107 sheath derive from an overlapping domain, evidenced by clonal sectors that mark both
108 sheath margins, with unmarked regions in between(*3,21*) (yellow-green-yellow sector,
109 Fig.3A). To clarify how overlap arises, we localized *CUC2* expression after primordium
110 emergence. Instead of a continuous ring (Fig.2M), we observed a diagonal line of
111 *CUC2* expression in the marginal domain, delimiting overlapping PZ ends (Fig.3B). In
112 *ns1/2* mutants the PZ had blunt ends delimited by *CUC2* (Fig.3C). Thus, *NS1/2* are
113 needed to extend the PZ and establish overlapping ends.
114 We incorporated these findings into a model for later developmental stages by
115 considering the primordium as a ring-shaped tissue with overlapping ends (Fig.3D).
116 Tissue was modelled as a sheet, with K_{PD} and K_{PER} corresponding to planar growth
117 rates, and K_{OP} to growth rate in sheet thickness. A clonal sector (yellow, Fig.3D) was
118 introduced to allow comparison with observed sectors.
119 Using similar growth patterns to those used above (Fig.S4) generated a sloping
120 primordium (Fig.3E cf. Fig.1H). K_{PD} and K_{PER} were modulated in the central, lateral
121 and marginal domains, leading to a wrapped primordium (Fig.3F cf. Fig.1I). SHEATH

identity was then introduced (Fig.3G cf. Fig.1J), consistent with the timing of sheath margin emergence (*3*, *4*), and further modulated growth rates. The result was a leaf with typical grass morphology and a yellow-green-yellow sector (Fig.3H cf. Fig.3A).

As a further test of the model, we removed marginal identity. The result was a more open primordium shape (Fig.3I-K), a mature leaf with a narrow sheath and proximal blade (Fig.3L), and a clonal sector marking a single sheath margin; all features observed experimentally in *ns1/2* mutants (*20*, *21*).

Taken together, our findings suggest two roles for *NS1/2* in the marginal domain: (1) Extension of the PZ and midplane to encircle the meristem and (2) Promotion of growth perpendicular to the midplane to drive primordium emergence and planar growth, shaped through differential regulation of K_{PD} and K_{PER}.

To explore the relationship between grass and eudicot leaves, we modified the grass models to produce a eudicot leaf, effectively reversing the steps taken during evolution. In the eudicot *Arabidopsis PRESSED FLOWER (PRS)* is the orthologue of maize *NS1/2. prs* mutants lack stipules, and *wox1* mutations enhance this phenotype to produce narrow leaves (*26*, *27*). 3D image analysis showed that stipules emerge later in marginal positions in wild-type leaves (as previously shown by live imaging (*28*)), and early *prs/wox1* primordia are narrower than wild type (Fig.S9). We therefore modelled the eudicot leaf primordium by contracting the PZ to a fraction of the apical circumference (Fig.4A-C), assigning stipule identity to the marginal domain, and creating an outer lateral domain(dark red Fig.4B-C). Growth patterns were specified in a similar manner to the grass leaf model but with modified distributions to generate a eudicot primordium (Fig.4D, Fig.S2I-J). The *prs* mutant was recapitulated by removing the marginal domain (Fig.4E-F), and *prs/wox1* by removing both the marginal and part of the outer lateral domains (Fig.4G-H).

147 To determine whether the model could also account for mutants which lack ad-
148 abaxial distinctions, we truncated the PZ to the central domain, replaced adaxial with
149 abaxial identity, and the midplane with an axial domain (Fig.4I-K). This led to a
150 radialised leaf, as observed in abaxialised mutants (Fig.4K)(*29*). Thus, ad-abaxial
151 genes may normally act to extend an axial domain to a midplane and promote planar
152 growth, supporting the idea that a midplane organizes the outgrowth of leaf blades
153 (*22*, *27*).
154 To simulate later stages of eudicot leaf development, we first modelled the
155 petiole-sheath hypothesis (Fig.1K) by increasing K_{PER} in the BLADE relative to
156 SHEATH. The result was a eudicot-like leaf, with SHEATH corresponding to petiole,
157 BLADE to lamina (Fig.4L-O). We next modelled the petiole-leaf hypothesis (Fig. 1I) by
158 subdividing the primordium domain fated to form the grass leaf tip (upper leaf zone)
159 into two subdomains (orange and purple, Fig.3E-H), and inhibiting K_{PAR} proximal to
160 this (Fig.S6). This generated a eudicot-like leaf (Fig.4P-S). In both models growth was
161 promoted in the marginal domain after primordium emergence but inhibited at the
162 marginal-lateral boundary leading to the formation of stipules (Fig.4O,S, Fig.S9).
163 Although both models can generate a eudicot leaf morphology, they make
164 different assumptions and predictions. The petiole-leaf hypothesis assumes additional
165 proximal-distal domains and is therefore less parsimonious. In addition, the petiole-
166 leaf hypothesis predicts petiole mainly derives from the middle of the early primordium
167 (orange, Fig.4S), whereas the petiole-sheath hypothesis predicts petiole derives from
168 the primordium base (Fig.4O). Live imaging supports the petiole-sheath prediction(*30*,
169 *31*). The petiole-leaf hypothesis predicts the *prs/wox1* mutant has a narrow petiole
170 base (Fig.4V), whereas the petiole-sheath hypothesis predicts a narrow petiole and
171 lamina (Fig.4U) as is observed. The petiole-leaf hypothesis further predicts that

172 homologues of petiole identity genes act throughout the grass leaf, except the tip,
173 whereas the petiole-sheath hypothesis predicts sheath-specific activity. Grass
174 homologues of the *Arabidopsis* petiole identity gene *BLADE ON PETIOLE (BOP)* are
175 expressed in the sheath, and expression stops at the sheath-blade boundary when
176 this becomes morphologically evident (Fig. 4W, (*32*, *33*)), and rice triple knock-out *bop*
177 mutants affect sheath, but not blade development (*32*, *33*). Taken together, these
178 findings strongly support the petiole-sheath hypothesis.

179 We show how a common ground plan of identities may modulate specified
180 growth to produce eudicot or grass leaf morphogenesis. In eudicots, *WOX* genes act
181 redundantly to extend the PZ and promote leaf and stipule planar growth (*27*, *34*, *35*).
182 The pattern of redundancy may vary among eudicot species, as tobacco mutants in
183 the *PRS* orthologue have very narrow leaves(*36*) instead of lacking stipules. A key
184 step in grass evolution was extension of primordium identity and *WOX* activity along
185 the ad-abaxial boundary to encircle the apex, driving primordium emergence and
186 planar growth. Further modulation of planar growth in the petiole and lamina domains
187 led to grass sheath and blade morphogenesis respectively, consistent with the 19th
188 century view of homology (Fig.1K). Other anatomical traits, such as venation patterns,
189 may represent further elaborations rather than being primary indicators of homology.
190 Our findings are comparable to those from animal Evo-Devo studies, where a
191 discarded hypothesis - the notion that the ventral side of insects corresponds to the
192 dorsal sides of vertebrates - was reinstated in the light of fresh developmental genetic
193 evidence (*37*). We further provide a mechanistic link between developmental genes
194 involved and their morphogenetic effects.
195

References

1. D. R. Kaplan, The problem of leaf morphology and evolution in the monocotyledons. *Q. Rev. Biol.* **48**, 437–457 (1973).
2. P. F. Stevens, Angiosperm Phylogeny Website. Version 13. *Angiosperm Phylogeny Website. Version 13.* (2016).
3. R. Johnston, S. Leiboff, M. J. Scanlon, Ontogeny of the sheathing leaf base in maize (Zea mays). *New Phytol.* **205**, 306–315 (2015).
4. B. C. Sharman, Developmental anatomy of the shoot of Zea mays L. *Ann. Bot.* **6**, 245–282 (1942).
5. A. M. Grey, No. *Bot. Textb.* **New York,** (1850).
6. A. Arber, The phyllode theory of the monocotyledonous leaf, with special reference to anatomical evidence. *Ann. Bot.* **32**, 465–501 (1918).
7. A. R. Arber, *Monocotyledons: a morphological study* (CUP Archive, 1925).
8. G. Henslow, The origin of monocotyledons from dicotyledons, through self-adaptation to a moist or aquatic habit. *Ann. Bot.* **25**, 717–744 (1911).
9. D. Candolle, A. P, *Organographie vegetale* (1827).
10. W. Troll, Die morphologische Natur der Karpelle. *Chron. bot*. **5**, 38–41 (1939).
11. F. Knoll, Bau, Entwicklung und morphologische Bedeutung unifazialer Vorläuferspitzen an Monokotylenblättern. *Österreichische Bot. Zeitschrift*. **95**, 163–193 (1948).
12. W. Hagemann, Studien zur Entwicklungsgeschichte der Angiospermenblatter, Ein Beitrag zur Klarung ihres Gestaltungsprinzips. *Bot Jahrbucher* (1970).
13. D. R. Kaplan, Comparative foliar histogenesis in Acorus calamus and its bearing on the phyllode theory of monocotyledonous leaves. *Am. J. Bot.* **57**, 331–361 (1970).

14. A. W. Eichler, *Zur Entwickelungsgeschichte des Blattes mit besonderer Berücksichtigung der Nebenblatt-Bildungen* (Elwert'sche Universitäts-Buchhandlung, 1861).
15. D. Jackson, B. Veit, S. Hake, Expression of maize KNOTTED1 related homeobox genes in the shoot apical meristem predicts patterns of morphogenesis in the vegetative shoot. *Development*. **120**, 405–413 (1994).
16. M. T. Juarez, R. W. Twigg, M. C. P. Timmermans, Specification of adaxial cell fate during maize leaf development. *Development*. **131**, 4533–4544 (2004).
17. F. T. S. Nogueira, D. H. Chitwood, S. Madi, K. Ohtsu, P. S. Schnable, M. J. Scanlon, M. C. P. Timmermans, Regulation of small RNA accumulation in the maize shoot apex. *PLoS Genet*. **5**, e1000320 (2009).
18. A. Hay, S. Hake, The dominant mutant Wavy auricle in blade1 disrupts patterning in a lateral domain of the maize leaf. *Plant Physiol.* **135**, 300–308 (2004).
19. J. Nardmann, J. Ji, W. Werr, M. J. Scanlon, The maize duplicate genes narrow sheath1 and narrow sheath2 encode a conserved homeobox gene function in a lateral domain of shoot apical meristems. *Development*. **131**, 2827–2839 (2004).
20. M. J. Scanlon, R. G. Schneeberger, M. Freeling, The maize mutant narrow sheath fails to establish leaf margin identity in a meristematic domain. *Development*. **122**, 1683–1691 (1996).
21. M. J. Scanlon, M. Freeling, Clonal sectors reveal that a specific meristematic domain is not utilized in the maize mutantnarrow sheath. *Dev. Biol.* **182**, 52–66 (1997).
22. C. D. Whitewoods, B. Gonçalves, J. Cheng, M. Cui, R. Kennaway, K. Lee, C.

Bushell, M. Yu, C. Piao, E. Coen, Evolution of carnivorous traps from planar leaves through simple shifts in gene expression. *Science (80-.).* **367**, 91–96 (2020).

23. D. L. O'Connor, A. Runions, A. Sluis, J. Bragg, J. P. Vogel, P. Prusinkiewicz, S. Hake, A division in PIN-mediated auxin patterning during organ initiation in grasses. *PLoS Comput Biol*. **10**, e1003447 (2014).

24. A. Richardson, A. B. Rebocho, E. Coen, Ectopic KNOX expression affects plant development by altering tissue cell polarity and identity. *Plant Cell*. **28** (2016), doi:10.1105/tpc.16.00284.

25. M. Aida, T. Ishida, M. Tasaka, Shoot apical meristem and cotyledon formation during Arabidopsis embryogenesis: interaction among the CUP-SHAPED COTYLEDON and SHOOT MERISTEMLESS genes. *Development*. **126**, 1563–1570 (1999).

26. N. Matsumoto, K. Okada, A homeobox gene, PRESSED FLOWER, regulates lateral axis-dependent development of Arabidopsis flowers. *Genes Dev.* **15**, 3355–3364 (2001).

27. M. Nakata, N. Matsumoto, R. Tsugeki, E. Rikirsch, T. Laux, K. Okada, Roles of the Middle Domain–Specific WUSCHEL-RELATED HOMEOBOX Genes in Early Development of Leaves in Arabidopsis. *Plant Cell*. **24**, 519–535 (2012).

28. M. Zhongjuan Zhang, Adam Runions, Remco A. Mentink, Daniel Kierzkowski, Michal Karady, Babak Hashemi, Peter Huijser, Sören Strauss, Xiangchao Gan, Karin Ljung and Tsiantis, A WOX/auxin biosynthesis module controls growth to shape leaf form. *Curr. Biol.* (2020).

29. M. E. Byrne, Networks in leaf development. *Curr. Opin. Plant Biol.* **8**, 59–66 (2005).

30. S. Fox, P. Southam, F. Pantin, R. Kennaway, S. Robinson, G. Castorina, Y. E. Sánchez-Corrales, R. Sablowski, J. Chan, V. Grieneisen, Spatiotemporal coordination of cell division and growth during organ morphogenesis. *PLoS Biol.* **16**, e2005952 (2018).

31. D. Kierzkowski, A. Runions, F. Vuolo, S. Strauss, R. Lymbouridou, A.-L. Routier-Kierzkowska, D. Wilson-Sánchez, H. Jenke, C. Galinha, G. Mosca, A growth-based framework for leaf shape development and diversity. *Cell*. **177**, 1405–1418 (2019).

32. Z. Dong, W. Li, E. Unger-Wallace, J. Yang, E. Vollbrecht, G. Chuck, Ideal crop plant architecture is mediated by tassels replace upper ears1, a BTB/POZ ankyrin repeat gene directly targeted by TEOSINTE BRANCHED1. *Proc. Natl. Acad. Sci.* **114**, E8656–E8664 (2017).

33. T. Toriba, H. Tokunaga, T. Shiga, F. Nie, S. Naramoto, E. Honda, K. Tanaka, T. Taji, J.-I. Itoh, J. Kyozuka, BLADE-ON-PETIOLE genes temporally and developmentally regulate the sheath to blade ratio of rice leaves. *Nat. Commun.* **10**, 1–13 (2019).

34. Z. Zhang, A. Runions, R. A. Mentink, D. Kierzkowski, M. Karady, B. Hashemi, P. Huijser, S. Strauss, X. Gan, K. Ljung, A WOX/Auxin Biosynthesis Module Controls Growth to Shape Leaf Form. *Curr. Biol.* (2020).

35. M. Vandenbussche, A. Horstman, J. Zethof, R. Koes, A. S. Rijpkema, T. Gerats, Differential recruitment of WOX transcription factors for lateral development and organ fusion in Petunia and Arabidopsis. *Plant Cell*. **21**, 2269–2283 (2009).

36. H. Lin, L. Niu, N. A. McHale, M. Ohme-Takagi, K. S. Mysore, M. Tadege, Evolutionarily conserved repressive activity of WOX proteins mediates leaf

296 blade outgrowth and floral organ development in plants. *Proc. Natl. Acad. Sci.*
297 **110**, 366–371 (2013).
298 37. J. I. Pueyo, J. P. Couso, Parallels between the proximal–distal development of
299 vertebrate and arthropod appendages: homology without an ancestor? *Curr.*
300 *Opin. Genet. Dev.* **15**, 439–446 (2005).
301 38. L. Conti, D. Bradley, TERMINAL FLOWER1 is a mobile signal controlling
302 Arabidopsis architecture. *Plant Cell*. **19**, 767–778 (2007).
303 39. J. Schindelin, I. Arganda-Carreras, E. Frise, V. Kaynig, M. Longair, T.
304 Pietzsch, S. Preibisch, C. Rueden, S. Saalfeld, B. Schmid, Fiji: an open-source
305 platform for biological-image analysis. *Nat. Methods*. **9**, 676–682 (2012).
306 40. A. Limaye, in *Developments in X-ray Tomography VIII* (International Society
307 for Optics and Photonics, 2012), vol. 8506, p. 85060X.
308 41. R. Johnston, M. Wang, Q. Sun, A. W. Sylvester, S. Hake, M. J. Scanlon,
309 Transcriptomic analyses indicate that maize ligule development recapitulates
310 gene expression patterns that occur during lateral organ initiation. *Plant Cell*.
311 **26**, 4718–4732 (2014).
312 42. E. Truernit, H. Bauby, B. Dubreucq, O. Grandjean, J. Runions, J. Barthélémy,
313 J.-C. Palauqui, High-resolution whole-mount imaging of three-dimensional
314 tissue organization and gene expression enables the study of phloem
315 development and structure in Arabidopsis. *Plant Cell*. **20**, 1494–1503 (2008).
316 43. E. Vollbrecht, L. Reiser, S. Hake, Shoot meristem size is dependent on inbred
317 background and presence of the maize homeobox gene, knotted1.
318 *Development*. **127**, 3161–3172 (2000).
319 44. E. E. Kuchen, S. Fox, P. B. De Reuille, R. Kennaway, S. Bensmihen, J.
320 Avondo, G. M. Calder, P. Southam, S. Robinson, A. Bangham, Generation of

leaf shape through early patterns of growth and tissue polarity. *Science (80-.).* **335**, 1092–1096 (2012).

Acknowledgements

We thank Devin O'Connor, the Coen Lab, Chris Whitewoods, the Hake Lab, Samuel Leiboff, China Lunde Shaw, and Andrew Hudson, for their support and helpful discussions. We thank Thai Dao for help with the PI staining and tissue clearing method. We also thank the microscopy and greenhouse staff at the JIC and the USDA and the Cornell Institute of Biotechnology's Imaging Facility. **Funding:** Funding for this project was provided by a bilateral NSF/BIO-BBSRC grant (BB/M023117/1) awarded to S.H. and E.C. BBSRC grants (BBS/E/J/000PR9787, BBS/E/J/00000152, BB/L008920/1, BBS/E/J/000PR9789) awarded to E.C. NSF grant (DEB-1457070) awarded to MS. HK received funding from the Chinese Academy of Sciences grants (XDB27010304 and ZDBS-LY-SM022) for JC. AR is funded by the University of Edinburgh Start-up funds. The Cornell Institute of Biotechnology's Imaging Facility is supported by NYSTEM (C29155) and NIH (S10OD018516) **Author contributions:** AER, EC, MS and SH wrote the manuscript. AER carried out immunolocalisations and *in situs*. AER, JC and EC developed the models. RJ carried out *in situs*. RK provided help with the modelling. BC carried out the confocal imaging of the Arabidopsis leaf primordia. AER, ABR, RJ, MS, SH, EC developed the project. SH, MS, EC, AR and HK provided funding. **Competing interests:** The authors declare no competing interests. **Data and materials availability:** Microscopy data is available via the Edinburgh University Datashare. All materials are available on request from the corresponding authors. The growing polarized tissue framework (GFtbox) software is freely available at:

https://sourceforge.net/projects/gftbox/files/ . The computational model codes are available via Github at: https://github.com/ThePlantShapeLab/Evolution-of-the-grass-leaf-by-primordium-extension-and-petiole-lamina-remodeling-

Supplementary Materials

Materials and Methods

Supplementary Text: Model Descriptions

Figs. S1 to S9

Tables S1 to S4

Movies S1 to S7

References (38-44)

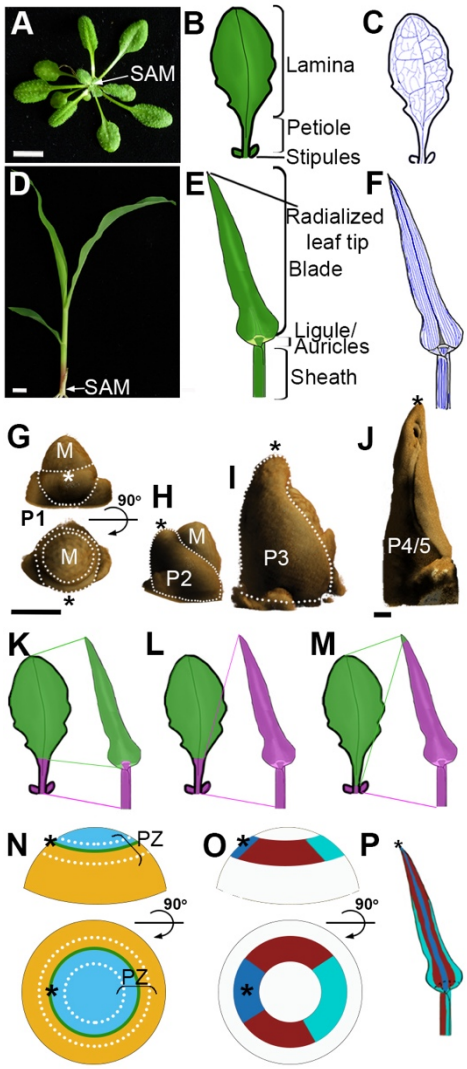

Fig. 1. Eudicot and grass leaf

(**A-F**) Eudicot *Arabidopsis thaliana*(A-C) and grass *Zea mays*(D-F). (A,D)Seedlings. Shoot apical meristem (SAM) position: arrow. Scalebar:1cm. Mature leaf morphology(B,E). Venation patterns(C-F). (**G-J**) Optical projection tomography of maize leaf primordia. P1 viewed from side or rotated 90º (top-down view)(J). P2 and P3 from side(K-L). P4/P5 with wrapped margins (front view, M). Meristem: M. Primordium: dotted line. Scalebar:100μm. (**K-M**) Proposed homologies between eudicot and grass leaves. (**N-P**) Domains in the grass leaf primordium. Primordial zone(PZ, dotted line) encircles the meristem, and straddles the boundary(green) between the abaxial(orange) and adaxial(blue) domains(N). Central(blue),

lateral(red), marginal(cyan) domains in the PZ(O) and the mature leaf(P) (modified from (*18*)). Midvein tip(*).

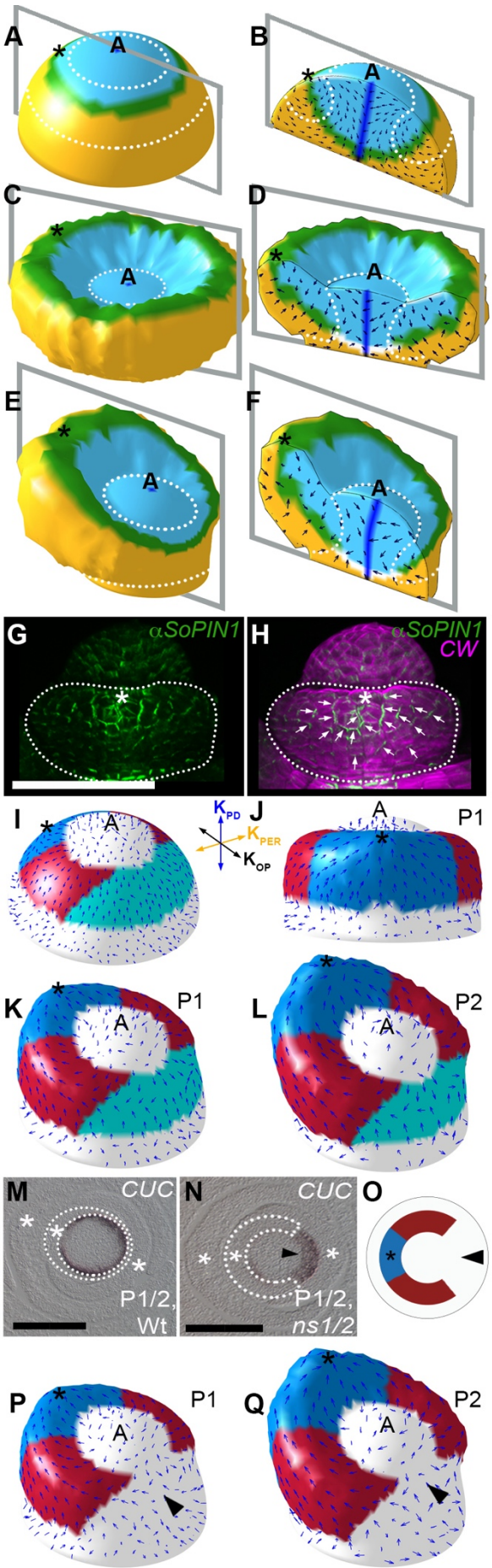
A
B
C
D
E
F
G
αSoPIN1
H
αSoPIN1
CW
I
J
P1
K
P1
L
P2
M
CUC
P1/2,
Wt
N
CUC
P1/2,
ns1/2
O
P
P1
Q
P2

Fig. 2. Grass leaf primordium emergence models

(**A**) Meristem apex with a pre-pattern of abaxial (orange) and adaxial (blue) identities. Primordial zone (PZ, dotted line) straddles the abaxial-adaxial midplane (green). (**B**) Section through (A). Orthoplanar polarity (black arrows) runs from the surface towards midplane and axial (dark blue) domains. (**C-D**) Fate of (A) if specified growth rate in PZ is high perpendicular to orthoplanar polarity. (**E-F**) As (C-D) but with specified growth rate increasing towards the midvein. (**G-H**) Whole-mount immunolocalisation of SoPIN1 (green) in barley P1/P2 primordia without (G) or with (H) cell wall signal (CW, magenta). SoPIN1 polarity: white arrows. (n=4) (**I**) Central (blue), lateral (red) and marginal (cyan) domains. Proximodistal (PD) field (blue arrows) runs from the PZ boundary towards the midvein tip (*) and apex (A). Axes illustrate specified growth rate orientations. (**J-L**) Model output at P1 (rear J, or oblique K, views) and P2 (L). (**M-N**) *ZmCUC2 in situ* hybridization in transverse sections of wildtype (M) and *narrowsheath1/2* (N) vegetative maize meristems (n=4). Primordium: dotted line. (**O**) *ns1/2* domains. (**P-Q**) PZ truncation by marginal domain removal (arrowhead). Scalebars:100μm.

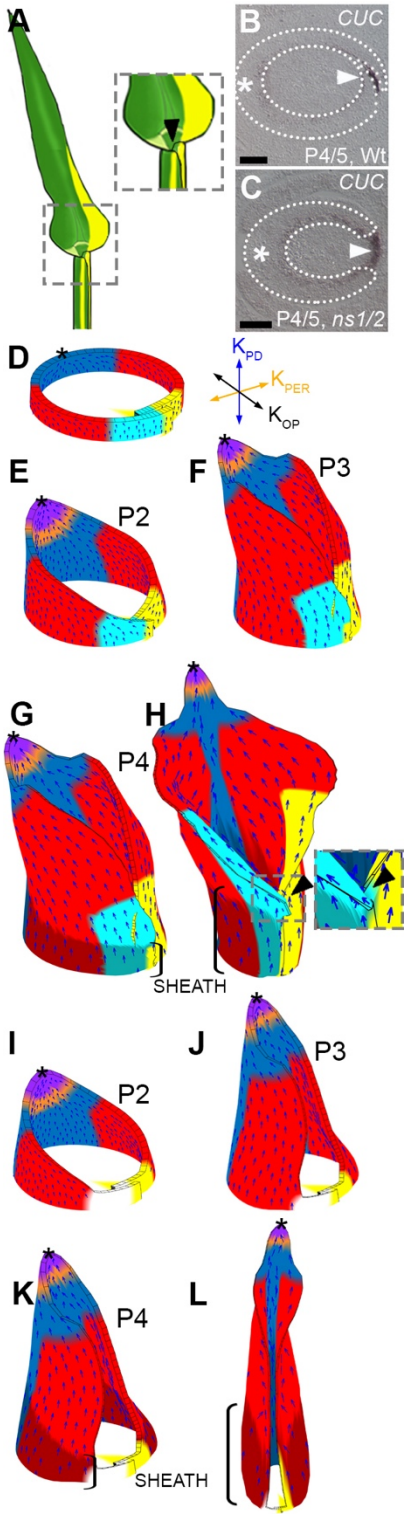

Fig. 3: Grass leaf tissue sheet model

(**A**) Single clonal sector (yellow) can mark both margins of the leaf with an intervening unmarked region (green, arrowhead, adapted from (*21*)). Box enlarged on right. (**B-C**) *ZmCUC2 in situ* hybridization in transverse sections of wildtype(B) and

narrowsheath1/2(C) vegetative maize meristems (n=4). P4/5: dotted line. Sheath margin: arrowhead. Scalebars:100μm. (**D-L**) Tissue sheet model. Initial ring with overlapping margins intersected by a clonal sector (yellow, D). Primordial zone(PZ) has central(blue), lateral(red) and marginal(cyan) domains. Proximodistal(PD) polarity(blue arrows) runs from the PZ boundary towards the midvein tip(*). Axes illustrate specified growth rates. Upper leaf domain (proximal- orange, distal- purple). Model output at P2(E) and P3(F). SHEATH identity (dark overlay and bracket) introduced at P4(G). (H) Final output with the sector marking both margins with intervening unmarked region (arrowhead). The contribution of the marginal domain to the blade is under-represented as the model maturation is accelerated compared to a real grass leaf. (**I-L**) Marginal domain removal generates a non-wrapping primordium(J-K), and a narrow-sheathed leaf with the sector marking one sheath margin(L).

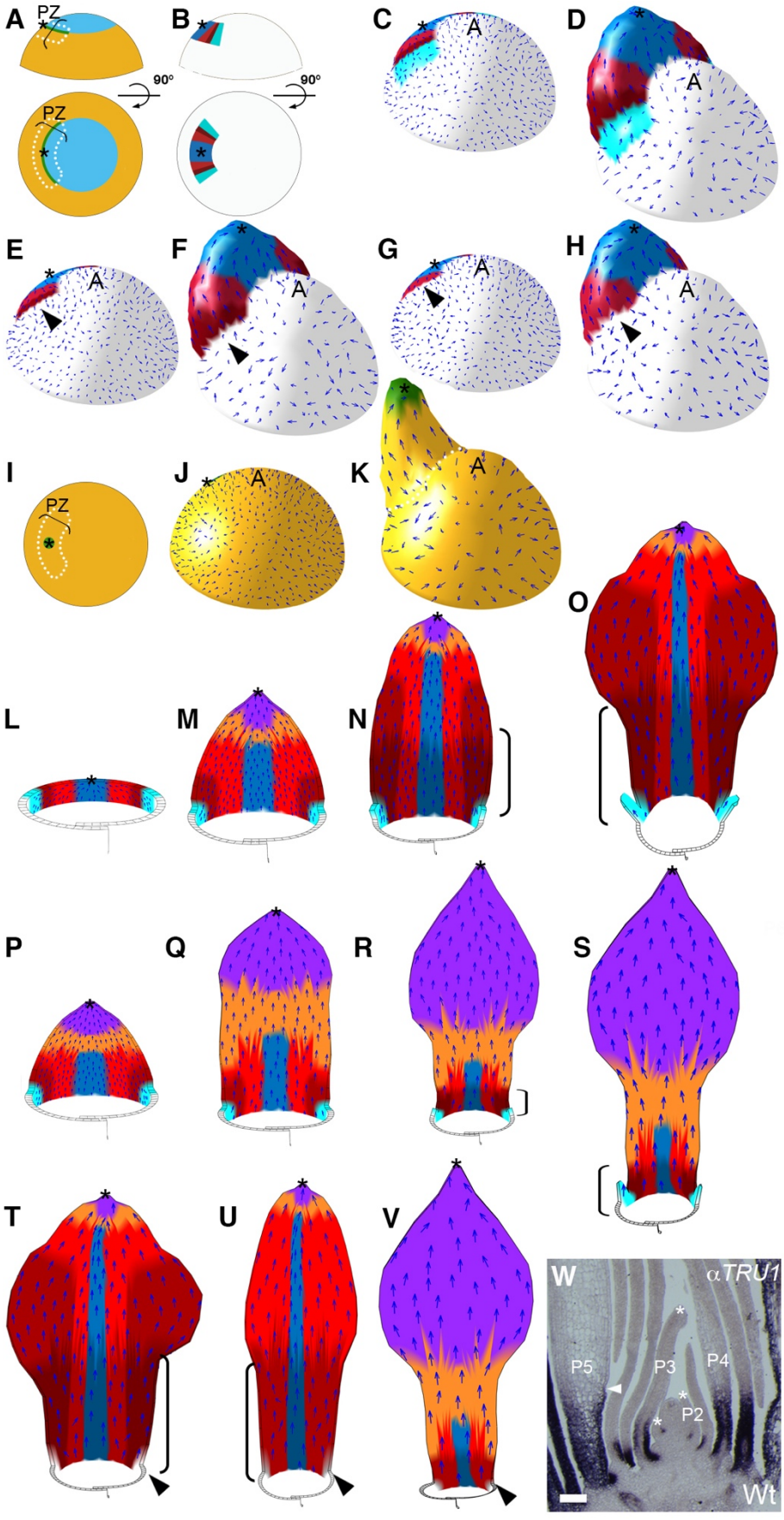

411

412 **Fig. 4: Eudicot leaf models**

(**A-B**) Eudicot leaf primordium domains. Primordial zone (PZ, dotted line) straddles the midplane (green) between the abaxial (orange) and adaxial (blue) domains (A). Central (blue), lateral (light red), outer lateral (dark red), marginal (cyan) domains in the PZ (B). (**C-G**) Volumetric primordium emergence models, with the proximodistal (PD) polarity field (blue arrows). midvein tip (*) apex (A). Wild-type (C-D), *prs* (E-F) and *prs/wox1* mutants (G-H). Arrowhead: missing domains. (**I-K**) Abaxialised mutant, (restricted PZ to central domain, and axial midplane) with a radialised primordium. (**L-V**) Eudicot leaf tissue sheet models. PD polarity runs from the PZ boundary towards the midvein tip. Putative proximal upper leaf (PUL, orange) and distal upper leaf (DUL, purple) domains. Asymmetries in leaf shape arise from the initial ring having overlapping ends and fluctuations from mesh subdivision. (**L-O**) Petiole-sheath hypothesis. (**P-S**) Petiole-leaf hypothesis. Model output at P2 (M, P-Q). SHEATH identity (dark gray overlay, bracket) introduced at P4 (N, R). Final output (O,S). (T) *prs* mutant in the petiole-sheath model (loss of marginal). (**U-V**) Marginal and outer lateral domain truncation generates a narrow primordium a narrow lamina leaf in the petiole-sheath model (U), but not the petiole-leaf model (V). (**S**) ZmTRU1 immunolocalisation in a maize vegetative shoot apex longitudinal section (n=4). Ligule: arrowhead. Leaf primordia plastochrons: P1-P6. Scalebar:100μm.

Science
AAAS

Supplementary Materials for

Evolution of the grass leaf by primordium extension and petiole-lamina remodeling

A. E. Richardson[1,2,3†*], J. Cheng[1,4,5], R. Johnston[6,7], R. Kennaway[1], Brianne R. Conlon[6], A.B. Rebocho[1], H. Kong[4,5], M. J. Scanlon[6*], S. Hake[2], E. Coen[1*]

[1] John Innes Centre, Norwich Research Park, Colney Lane, Norwich, NR4 7UH.

[2] ARS/USDA Plant Gene Expression Center, 800 Buchanan Street, Albany, 94710.

[3†] Institute of Molecular Plant Science, School of Biological Sciences, University of Edinburgh, Kings Buildings, Max Bourne Crescent, Edinburgh, EH9 3BF.

[4] State Key Laboratory of Systematic and Evolutionary Botany, CAS Center for Excellence in Molecular Plant Sciences, Institute of Botany, Chinese Academy of Sciences, Beijing 100093, China.

[5]College of Life Sciences, University of Chinese Academy of Sciences, Beijing 100049, China.

[6] Plant Biology Section, School of Integrative Plant Science, Cornell University, Ithaca, NY14853.

[7] The Elshire Group Limited, Palmerston North 4472, New Zealand.

[†]Current address

Correspondence to: annis.richardson@ed.ac.uk, mjs298@cornell.edu, enrico.coen@jic.ac.uk

454 **This PDF file includes:**

455 Materials and Methods

456 Supplementary Text: Model Descriptions

457 Figs. S1 to S9

458 Tables S1 to S4

459 Captions for Movies S1 to S7

460 References (38-44)

461

462 **Other Supplementary Materials for this manuscript include the following:**

463 Movies S1 to S7

464

Materials and Methods

Antibodies

The TRU1 primary antibody, was provided by the Chuck lab (*32*), and used at a 1:400 dilution. The SoPIN1 primary antibody was provided by Devin O'Connor and the Hake lab (*23*) and used at a 1:200 dilution. Standard anti-guinea pig-Alkaline Phosphatase conjugated secondary antibodies (Sigma Aldrich, A5062) were used in the TRU1 immunolocalisation experiments at a 1:400 dilution. Standard anti-guinea pig-Alexa488 secondary antibodies from Life Technologies (A11073,lot 1235789) were used in the SoPIN1 immunolocalisation experiments, at a 1:200 dilution.

Immunolocalisation

Maize vegetative shoots were fixed in 4% PFA/ 0.1% DMSO/ 0.1% Triton-X100 overnight, before embedding in paraplast plus. 10μm sections were mounted on Probe on Plus slides (Fisher Scientific) on water and dried overnight on at 37°C. Immunolocalisation of KN1 was carried out on the sectioned tissue based on the method described in (*38*) . The method is briefly outlined here. Sections were dewaxed in histoclear (National Diagnostics), then rehydrated through a descending ethanol series (100%, 100%, 95%, 85%, 70%, 50%, 30%, water). Slides were then vigorously boiled in 10mM citrate solution, pH6 for 10mins. Once cooled, slides were washed in PBS, then blocked in 1% BSA in PBS and 0.3% Triton-X100 for 3 hours. Slides were then washed in PBS, and incubated in primary antibody in 1% BSA in PBS, overnight at 4°C. Slides were washed three times in PBS/0.3% Triton-X100 and once with PBS, then incubated in secondary antibody in 1% BSA in PBS for 2 hours at room temperature. Once complete, slides were washed three times in PBS/0.3% Triton-X100 and once with PBS, then incubated in 0.05M $MgCl_2$/TBS, pH9.5. To visualize

the antibody localization, slides were incubated in 5-bromo-4-chloro-3-indolyl phosphate (BCIP)/ nitroblue tetrazolium (NBT) mix (Roche, #11681451001) in 0.05M $MgCl_2$/TBS, pH9.5 to develop dark precipitate signal (~30mins-1hour). The precipitation reaction was stopped through rinsing with deionized water. Slides were then imaged on a Leica dissecting microscope under water in brightfield conditions.

Tissues incubated with anti-SoPIN1 were stained for 20 minutes in 0.1% calcofluor (fluorescent brightener 28, Sigma-Aldrich #F3543), washed and mounted in water and imaged on a Leica SP8 confocal microscope. The subcellular localization of SoPIN1 was assessed in relation to the calcofluor cell wall stain using FIJI(*39*).

Wholemount Immunolocalisation

Barley vegetative meristems with different stage leaf primordia attached were dissected from seedlings when the 3rd leaf was emerging, then fixed in FAA (50% ethanol, 5% acetic acid, 3.7% formaldehyde (Sigma Aldrich)) with 1% DMSO and 0.5% Triton-X100, placed under vacuum (at least 25Hg) for 3 replicates of 10mins, then fixed overnight at 4°C. Whole-mount immunolocalisation of SoPIN1, and subsequent calcofluor white staining of the cell walls, was carried out as described previously in (*24*). Samples were stored in PBS, and imaged under PBS on a Leica SP5 (II) confocal microscope using a x25 dipping lens (Calcofluor, violet laser diode, 405nm excitation laser, and PMT detectors, 400-480nm; Alexa-488, argon ion, 488nm excitation laser and PMT detectors 500-575nm). Z-stack images of the meristems and leaf primordia, where analysed using FIJI (*39*). The subcellular localisation of SoPIN1 relative to the calcofluor cell wall stain was analysed by hand in FIJI and a white arrow was added to indicate localization orientation.

Optical Projection Tomography

Maize shoot apexes were dissected from 2-week-old B73 seedlings, and fixed in 100% ethanol. These were further dissected under 100% ethanol to the desired primordium stage, and then stained with propidium iodide using the following protocol. Samples were fixed in 100% ethanol overnight, then rehydrated to 80% ethanol before boiling at 80°C for 12 minutes. Gradual rehydration was then completed to water, and the samples were incubated for 12 hours with alpha-amylase solution (20mM Sodium phosphate buffer (pH7), 2mM NaCl, 0.25mM $CaCl_2$, 0.3mg/ml alpha-amylase from *Bacillus licheniformis* (Sigma Aldrich A4551)) at 37°C. The samples were then washed in water and incubated with 1% periodic acid (Sigma Aldrich, 3951) for 1 hour. Once completed the samples were washed in water and incubated in Schiff Reagent (PI) (100mM sodium metabisulphite and 0.15M HCl; propidium iodide to a final concentration of 100 mg/mL) for 2 hours. Final samples were washed in water and mounted in low melting point agarose, cut to a prism shape, and cleared in BABB (2: 1 benzyl benzoate: benzyl alcohol). Imaging was carried out on the Coen lab prototype OPT microscope as described in(*24*). Images were taken at 400 angles, using white light through the GFP1 filter, and UV light through the GFP1 and TXR filters. The images were aligned using NRecon (NRecon, version 1.6.3.3; SkyScan 2010) and reconstructed and visualized using Drishtii (*40*).

Image Processing

Figures were assembled using Adobe Photoshop, with standardized scale bars and added annotations. All images shown are representative of more than 3 biological replicates.

In situ **Hybridisation**

Antisense probes targeted to *ZmCUC2* (GRMZM2G139701) mRNA (primers: CUC2-F1 TACCATTTCCTCCCCAGCTC, CUC2-R1 GAACGACGACCCAGTCACTT). *In situ* hybridization was carried out as in (*41*) outlined here in brief. Tissue was deparaffinised using histoclear, then rehydrated through an ethanol series. Samples were digested using 100μg/mL pronase (Sigma-Aldrich #P6611) in 100mMTris/5mM EDTA, pH7.5, for 30minutes at 37°C. Digestion was stopped by the addition of 0.2% glycine before washing and re-fixing in 4% formaldehyde/PBS for 10minutes. Slides were then treated in 0.1M Triethanolamine-HCl / 0.5% Acetic Anhydride (Sigma-Aldrich #320102) for 10 minutes before dehydrating through an ethanol series. Tissue was incubated overnight with the probes at a 1:100 dilution in hybridisation buffer (0.375M NaCl, 12.5mM Tris-HCl pH8, 12.5mM Sodium Phosphate pH6.8, 6.25mM EDTA, 50% deionized formamide, 12.5% dextran sulfate, 1.25x Denhardt solution, 0.0125mg/mL tRNA) at 50°C. Slides were washed in 0.2x SSC at 55°C, then treated with RNAse (1:1000 dilution of 10mg/mL RNAse in 0.5M NaCl/10mM Tris/ 1mM EDTA, pH7.5) at 37°C for 30 minutes, before repeating the SSC washes. Slides were blocked in Roche Blocking Reagent (#11-096-176-001) for 30 minutes, washed in 1% BSA/0.3 % Triton-X100/TBS, and incubated at 4°C with a 1:1250 dilution of anti-Dioxigenin-AP Fab fragments (Roche, #11093274910) in 1% BSA/0.3 % Triton-X100/TBS overnight. Slides were then washed with in 1% BSA/0.3 % Triton-X100/TBS, then in 0.05M $MgCl_2$/TBS, pH9.5. To visualize the probe localisation, the tissue was incubated in 1:50 dilution of NBT/BCIP in 0.05M $MgCl_2$/TBS, pH9.5, until dark precipitate formed. The staining reaction was stopped by transferring to TE buffer and the slides were imaged on a Leica MZ16F microscope with a Qimaging Micropublisher camera under water and brightfield conditions.

Primordium Measurements

Wild type Columbia (Col) and *prs/wox1* (from Yuling Jiao, Chinese Academy of Sciences) double mutant (Col) Arabidopsis seed were sterilized and plated, then cold-stratified at 4°C for at least 4 days on MS plates (1xMurashige and Skoog Basal Salts, 1xGambourg's vitamins, 0.8% sucrose, 0.5 mM MES, 0.3% Gelzan). Plates were moved to growth chambers under long day conditions (22°C, 50% humidity, 16 hours at 100 µmols light). 12-14 days later, cotyledons, large early leaves, and roots were dissected off, and seedlings were fixed overnight in ice cold FAA (3.7% formalin, 5% acetic acid and 50% ethanol, EtOH), then dehydrated to 100% EtOH for storage at 4°C.

Samples were stained with propidium iodide based on (*42*, *43*) as follows in brief. Seedlings were rehydrated to water, then stained with propidium iodide (1% periodic acid for 1 hour, then 10µg/mL propidium iodide in pseudo-Schiff buffer (100mM sodium metabisulphite, 0.15N HCl in water) overnight). To mount samples were dehydrated to 100% EtOH before clearing in methyl salicylate overnight at 4°C.

Cleared Arabidopsis shoot apical meristems (SAMs) and young leaf primordia were imaged at the Cornell Institute of Biotechnology's Imaging Facility using the Zeiss LSM880 confocal microscope on an inverted platform. PI staining was excited with the 514 nm argon laser, collecting an emission bandwidth between 539 and 735 nm through a C-Apochromat 40x/1.2 W Korr FCS M27 objective. Tissue was arranged in a longitudinal orientation (XY) and z-stacks were acquired as optical median sections through the SAM and young P1 and P2 leaf primordia. Z-stack slice interval was set to 1:1:1, x:y:z with a step size of 0.415 µmin all dimensions, and 16-bit images were obtained.

590 Image stacks were collected in .CZI format and then converted to .TIFF using FIJI
591 freeware. Stacks were then analyzed in VolView 3.2 (Kitware) via orthogonal
592 projections. For angle of insertion measurements (A_i), the tip of the SAM was marked
593 and maintained while traveling down XZ slices and served as the vertex of A_i. The two
594 arms of A_i connected the vertex (on the SAM) to the two edges of the leaf primordia
595 where it connected to the SAM. As the optical sectioning continued down the
596 orthogonal XZ slices, a white line between the SAM and the leaf primordia is observed
597 marking where the cell walls of the leaf primordia aligned with the cell walls at the edge
598 of the SAM. Measurements for A_i were taken below this point to only measure the
599 region where the leaf primordia attached to the SAM. For WT samples with stipules,
600 measurements on P2 include the emerging stipules. A_i measurements were taken on
601 alternating subsequent slices traveling down the XZ stack until the edges of leaf
602 primordia were too difficult to define. The final five measurements for a primordium in
603 a sample were averaged to represent the maximum angle of insertion, while
604 minimizing slice to slice variation. Data analysis was preformed using Microsoft Excel.
605 T-tests assuming equal variance were used to determine significant differences in A_i
606 for WT and *prs/wox1* double mutant samples.

Supplementary Text: Model Descriptions

Model Aims

The following models aim to broadly capture the morphology of the leaf primordium in grasses and eudicots at different stages of development by placing them in a common framework with a shared starting point (the apex for volumetric models and the ring for the sheet models). By developing the models, we aimed to clarify predictions of different hypotheses relating to leaf homology in the grass leaf and eudicot leaf, and highlight correspondences along the mediolateral axis in relation to genetic data. The models do not represent any particular grass or eudicot species, but try to capture key morphological transitions, potential gene functional domains and overall growth patterns in a generic manner.

Model Limitations

The models have several limitations. There is not attempt to match observed growth rates precisely where they are known (previously published models do this more effectively) but to provide patterns that are broadly consistent with observations. Later developmental stages are compressed for computational convenience, which again precludes precise alignment with experimental data. The models lack collision detection, which means that if two parts of the mesh collide they will pass through each other rather than providing mechanical feedback. Mechanical constraints from neighbouring leaves or from the encircled stem/apex, which might prevent the leaf from bending back, are therefore not present and there is no attempt to correctly capture the extent to which the leaf leans back at later stages. For similar reasons, the model may be more prone to buckling than is the case for real leaves.

Model Description

Models are constrained by the need to capture the main morphological transitions observed, while also incorporating the general observation that growth is mainly driven from proximal regions. Only local growth rates are specified and thus all changes in curvature (e.g. primordium emergence, wrapping) arise as emergent features through the mechanical constraints of tissue connectivity. We model generic grass and stipulate eudicot leaves and there is no attempt to precisely match quantitative values in either case. The aim is to clarify predictions different hypotheses make and evaluate them against experimental data.

All of the models covering the initiation (volumetric models), wrapping, and expansion stages of leaf development (sheet models) are implemented in Matlab using the freely available software GFtbox (http://sourceforge.net/projects/gftbox/). Full code for all models is available from Github.

In all models the tissue is treated as a continuous volume, in which each region has specified growth rates that define both the orientations and rates of growth it would undergo if in mechanical isolation. Resultant growth rates are those attained when the region is mechanically connected with the rest of the tissue. The differences between the specified and resultant growth rates is the residual strain. The deformation of the tissue is computed such that residual strain is minimised. After each step in the model residual strain is assumed to dissipate for the first three phases of growth, reflecting the irreversible nature of plant growth. For the final phase of the grass model, residual strain is retained as elastic forces may contribute to the opening of the leaf. While this is likely valid for much of primordium development, residual strains may accumulate during later stages of development as the tissue becomes stronger and less plastic.

The models are defined by two coordinated networks: the polarity regulatory network (PRN) which defines polarity fields, and the growth regulatory network (KRN) which defines specified growth rates. These networks are influenced by factors which can be defined as identity factors, denoted by i, or signalling factors denoted by s which can diffuse within the tissue during growth. Signalling factors diffuse according to the following equation, where x denotes the specific factor:

$$\partial S_x / \partial t = D_x \nabla^2 S_x - De_x S_x$$

Where D is the diffusion constant, De is the decay constant, and S is the concentration of the signalling factor.

Growth rates can be restricted to domains defined by these factors, or modulated by them. Growth rates can be promoted by factors, where promotion is specified by:

$pro(z, iX)$ or $pro(z, sX >= L)$

where iX denotes an identity factor, sX denotes a signalling factor, L denotes a threshold level, and z is the extent to which the factor promotes growth rate. pro denotes multiplication of the growth rate by $1+zX$. Growth rates can also be inhibited by factors, where inhibition is specified by:

$inh(z, iX)$ or $inh(z, sX >= L)$

where iX denotes an identity factor, sX denotes a signalling factor, L denotes a threshold level, and z is the extent to which the factor inhibits growth rate. inh denotes multiplication of the growth rate by $1/(1+zX)$.

Below we describe the KRNs for each model. We use boldface for vectors of values (each vector has one value per mesh vertex), and italic for scalar values. Multiplication of vectors is elementwise and indicated by an asterisk. Identity factors are assigned a value of 1 where they are expressed. The expression $(1\text{-}f_x)$ generates the complementary expression pattern for factor f_x. The expression $(s_x < t_{sX})$ indicates

vertices where factor s_x is less than a threshold value t_{sX}. General parameters are indicated by n_y, where y denotes the parameter index. Parameters related to the action of a signalling or identity factor are denoted by m_x, p_x, and h_x where x defines the factor the parameter relates to. m defines multiplication, p promotion, and h inhibition. All model parameters are listed in Tables S1 and S2.

Volumetric Models of Primordium Emergence (Fig.2, Fig.4C-K, Fig.S1, Fig.S2, Fig.S3)

The primordium emergence models are volumetric GFtbox models, based on a hemisphere shape (radius of 1, height of 1), with 64188 finite elements. Factors are set up from steps 0 to 3. This setup phase is followed by a single growth phase in which the identity factors define specified growth rates. All models have both an APEX factor (Fig.S1A, black) that defines the apex of the meristem and a PZ factor that defines the primordium (Fig.S1A, grey). The remaining factors in the model can be classified based on their distribution three axes: ad-adaxial, mediolateral, proximodistal (Fig.2, Fig.S1).

Growth orientations are defined relative to polarity fields. All models share a single orthoplanar polarity field which points from the surface of the hemisphere towards the MIDPLANE and the CORE identity regions. This field is required for outgrowth from the hemisphere (Fig.2B). The wildtype grass leaf, *narrowsheath* mutant, and eudicot models also share a second proximal-distal (PD) polarity field which points from the boundary of the PZ towards the midvein tip (Fig.2I).

In each model the identity factors illustrated in Fig.2 and Fig.S1 are used to modulate three specified growth rates. One growth rate (K_{OP}) is defined parallel to the orthoplanar polarity field. The other two growth rates are in the plane perpendicular to

the orthoplanar polarity field: K_{PD} is aligned with proximal distal polarity and K_{PER} is perpendicular to K_{PD} (and K_{OP}).

In all volumetric models, K_{OP} is set to a low level in the APEX domain and zero elsewhere. Growth perpendicular to the orthoplanar axis (K_{PD} and K_{PER}) are also at a constant low rate in the APEX domain. This growth rate pattern drives enlargement of the meristem apex. Common to all models, growth rates perpendicular to the orthoplanar polarity (K_{PD} and K_{PER}) are enhanced in the PZ domain (Fig.S2).

Formation of ring primordium (Fig.2C,D, Fig.S2A-D):

K_{OP} is low (zero except for a very low level in the APEX domain). K_{PD} and K_{PER} are high in the PZ and APEX domains. As there is no proximal distal polarity field in this model, K_{PD} and K_{PER} are equal:

$$\mathbf{K_{OP}} = m_{APEX} * \mathbf{i_{APEX}}$$

$$\mathbf{K_{PD}} = m_{APEX} * \mathbf{i_{APEX}} + m_{PZ} * \mathbf{i_{PZ}}$$

$$\mathbf{K_{PER}} = \mathbf{K_{PD}}$$

Formation of sloping ring primordium (Fig.2E-F, Fig.S2E-F):

Same as previous model except growth perpendicular to the orthoplanar polarity field is modulated by medio-lateral factors such that it is highest in CENTRAL, then LATERAL, and lowest in the MARGINAL domain. Growth is also inhibited by a graded factor from the margin, sPZMARGIN.

$$\mathbf{K_{OP}} = m_{APEX}\ \mathbf{i_{APEX}}$$

$$\mathbf{K_{PD}} = m_{APEX}\ \mathbf{i_{APEX}} + (m_{CENTRAL}\ \mathbf{i_{CENTRAL}} + m_{LATERAL}\ \mathbf{i_{LATERAL}} + m_{MARGINAL}\ \mathbf{i_{MARGINAL}}) * \mathbf{i_{PZ}} * \mathrm{inh}\ (h_{sPZMARGIN},\ \mathbf{s_{PZMARGIN}})$$

$\mathbf{K_{PER}} = \mathbf{K_{PD}}$

Leaf primordium models (Fig.2I-L, P-Q, Fig.4C-K, Fig.S2G-L):

Both the eudicot and grass primordium emergence models share the same KRN. In these models a proximal-distal polarity axis is introduced, allowing the separate specification of K_{PD} and K_{PER}. Proximodistal polarity converges on the midvein tip and therefore tends to orient circumferentially near the PZ rim and longitudinally further from the rim and centrally. To generate an upward growing primordium with a tip, K_{PER} is therefore enhanced through promotion by sRIM (Fig. S2H) and K_{PD} is enhanced in a complementary domain through restriction by sRIM (Fig. S2G). In addition, K_{PD} and K_{PER} are modulated mediolaterally, and is enhanced proximally (Fig.S2G) through restriction by sRIM. K_{PER} is also modulated mediolaterally (promoted by CENTRAL and LATERAL and inhibited by sPZMARGIN) to generate a mediolateral gradient in growth rates. K_{PD} and K_{PER} are also promoted by ABAXIAL to reduce bending back of the primordium. K_{PER} is inhibited by sTIP and sMID to prevent widening of the primordium tip

$$\mathbf{K_{OP}} = m_{APEX}\,\mathbf{i_{APEX}}$$

$$\mathbf{K_{PD}} = m_{APEX}\,\mathbf{i_{APEX}} + (m_{CENTRAL}\,\mathbf{i_{CENTRAL}} + m_{LATERAL}\,\mathbf{i_{LATERAL}} + m_{MARGINAL}\,\mathbf{i_{MARGINAL}}) * \mathbf{i_{PZ}} * \mathrm{inh}\,(h_{sPZMARGIN},\ \mathbf{s_{PZMARGIN}}) * \mathrm{pro}\,(p_{ABAXIAL},\ \mathbf{i_{ABAXIAL}}) * (n_1 + (\mathbf{s_{RIM}} < t_{sRIM}))$$

$$\mathbf{K_{PER}} = m_{APEX}\,\mathbf{i_{APEX}} + m_{CENTRAL.PZ}\,\mathbf{i_{CENTRAL}} * \mathbf{i_{PZ}} + m_{LATERAL.PZ}\,\mathbf{i_{LATERAL}} * \mathbf{i_{PZ}} * \mathrm{pro}\,(p_{sMID},\ (\mathbf{s_{MID}} < t_{sMID}) * \mathrm{pro}\,(p_{ABAXIAL},\ \mathbf{i_{ABAXIAL}}) * \mathrm{inh}\,(h_{sTIP},\ \mathbf{s_{TIP}}) * (\mathbf{s_{RIM}} < t_{sRIM})$$

757 * inh ($h_{sPZMARGIN}$, **SPZMARGIN**))

758 * inh (h_{sMID}, (**SMID** > t_{sMID}))

759

760 The *narrowsheath and prs* models are the same as the wildtype leaf models, except
761 MARGINAL is set to zero and the PZ is truncated by loss of the marginal domain. In
762 the *prs/wox1* mutant model MARGINAL and OLATERAL are set to zero and the PZ is
763 truncated by loss of both the MARGINAL domain and the outer part of the LATERAL
764 domain. The abaxialised mutant model is the same as wildtype, except ADAXIAL is
765 set to zero, ABAXIAL is expressed throughout, the PZ is restricted to the CENTRAL
766 domain, and the midplane is reduced to an axial domain.

767

768 **Tissue Sheet Models of Further Primordium Development (Fig.3, Fig.4)**

769 The sheet models are based on a ring-shaped canvas with overlapping edges. The
770 ring is 0.03mm high with a radius of 0.07mm and contains 5457 finite elements.
771 Factors are set up from timesteps 0 to 0.32. This setup phase is then followed by a
772 series of growth phases in which the identity factors modulate the specified growth
773 rates.

774 Most previous eudicot leaf models are held in a plane (*30*, *31*, *44*) and do not
775 address primordium emergence, or how curvature out of the plane is generated and
776 controlled. To model both the curvature and shape changes (emergent features)
777 during grass development we found that parameters and interactions needed to be
778 adjusted during different phases. The first phase is concerned with primordium
779 emergence. The second phase is when the edges of the primordium wrap around
780 each other. The third phase involves extension of the primordium through proximal
781 growth. The fourth phase involves unfolding of the grass primordium, and the fifth

involves further flattening of the grass leaf (there is no fourth or fifth phase for the eudicot leaf). Phase 4 for grasses is relatively short for convenience of modelling and would extend for much longer in a real grass leaf. Consequently, the contribution of proximal regions (e.g. the marginal domain) to the mature leaf is under-represented in the final stages of the model.

There are four phases in the grass leaf model:

- **Phase 1:** Steps 0.32 to 0.8, define growth from primordium initiation to the P2 stage of grass leaf development.
- **Phase 2:** Steps 0.8 to 1.15, define growth during the grass leaf primordium from P2 to P4, when the margins of the primordium overlap.
- **Phase 3:** Steps 1.15 to 1.25, define growth during sheath extension.
- **Phase 4:** Steps 1.25 to 1.4, define growth during unwrapping of the blade margins.

There are three phases in the eudicot leaf model:

- **Phase 1:** Steps 0.32 to 0.8, define growth from primordium initiation to P1/2.
- **Phase 2:** Steps 0.8 to 1.15, define a further period of primordium growth.
- **Phase 3:** Steps 1.15 to 1.35, define the final stages of growth.

All sheet models share a common pattern of identity factors. The canvas has two surfaces; A (adaxial) and B (abaxial); which can differentially influence growth rates. The rim of the canvas corresponds to the region near the adaxial/abaxial boundary in the volumetric models (Fig.S1, midplane). The canvas is separated into a primordial zone (PZ, grey, Fig.S3A) and base, which enables the fixation of the basal and overlapping nodes to simulate attachment to the stem. Identify factors can be classified based on their influence on two axes: mediolateral and proximodistal

807 (Fig.S3). To generate the grass leaf model the identity factor WRAPPER (Fig.S3F) is
808 used to modulate growth rates in the overlapping leaf margins. The grass models also
809 have an additional signalling factor sMARGINAL (Fig.S3E). These two factors are not
810 used in the eudicot models.

811 To generate the eudicot (Fig. 4) models, the size of the PZ domain is reduced
812 and mediolateral domains correspondingly compressed. The size of the outer-lateral
813 marginal domains was based on measurements on primordium sizes in *prs* and
814 *prs/wox* mutants (Fig.S9). The outer region of the LATERAL domain is defined as
815 OLATERAL. The MARGINAL domain is allocated a STIPULE identity, with a boundary
816 identity, STBOUND, between LATERAL and MARGINAL, which produces a signalling
817 factor sSTBOUND (Fig.S3I).

818 To generate the grass *narrowsheath* (Fig.3I-L), and the *prs* (Fig.4T) mutants
819 the MARGINAL domain is removed and the PZ truncated accordingly. For *prs/wox1*
820 mutants the MARGINAL domain is removed and the LATERAL domain is truncated
821 (Fig.4U).

822 KRNs give specified growth rates in the PZ domain defined relative to a
823 proximal-distal polarity field within the plane of the canvas, which orients from the base
824 towards the midvein tip (Fig.3D). K_{PD} is specified growth rate parallel to the polarity
825 and K_{PER} specified growth rate perpendicular to the polarity. Growth rates on the inner
826 adaxial (A) or outer abaxial (B) surface of the canvas are indicated by appending
827 letters A or B respectively. Specified growth in sheet thickness is defined by K_{NOR}
828 which is equivalent to K_{OP} in the volumetric models.

829 The upper leaf (UL) and lower leaf (LL) domains are introduced part-way
830 through phase 1 once the primordium has emerged from the ring (Fig.4P, timestep
831 0.7). To define the position of the UL and LL we tracked the tip of the mature grass

leaf model (Fig.3H) back to this early stage, and defined the UL and LL based on a threshold of sPROX. The same threshold value is then used to defined the UL and LL domains in the grass and petiole-leaf models. A slightly different threshold is used for the petiole-sheath model in which the UL domain has no functional role. The UL domain is further subdivided into the proximal UL (PUL, orange Fig.3, Fig.4) and the distal UL (DUL, purple Fig.3, Fig.4). Although these domains are marked in all models, they are only used to modulate the KRN in the petiole-leaf hypothesis models.

The SHEATH (Fig.3G, dark grey overlay and bracket) is introduced at the end of phase 2, such that SHEATH is activated where a graded proximodistal factor (sPROX, Fig.S3B in the grass models and sLEAFBASE, Fig.S3H, in the eudicot models) is above a threshold value. BLADE is throughout the PZ and is inhibited by SHEATH creating non-overlapping SHEATH/BLADE domains. Thus, in mutants which lack SHEATH identity (e.g. mutants in *BOP* homologues) SHEATH is replaced by BLADE (Fig.S8). The timing for establishing the SHEATH domain was chosen because the maize sheath margin does not grow until P3/P4, as is most evident from the region opposite the midvein where the overlapping sheath margins arise as shown by CT imaging (*3*). This is also the stage at which TRU1 protein localisation fully encircles the meristem (Fig. 4W). However, activation of SHEATH identity at a single stage is likely an oversimplification as TRU1 expression is detected first near the presumptive midrib and then extends towards the margin (Fig. 4W).

As few changes as possible were introduced to transition from the grass leaf to the eudicot model. However, because of the differing geometries, number of phases and sizes between eudicot and grass primordia, growth patterns typically had to be specified in different ways or with different parameters.

PHASE 1 Grass Model (Fig.3D-E, Fig.S4A-B)

The ring grows to form a sloping primordium. As with the volumetric primordium emergence model (Fig. S2G), K_{PD} is promoted proximally with rates declining mediolaterally(central-marginal) (Fig.S4A). K_{PER} is promoted in a complementary pattern by RIM and inhibited towards the limits of the central and marginal domains (Fig.S3B, Fig.S4B), again similar to the pattern for the volumetric primordium emergence model (Fig. S2H). Thus, resultant areal growth rates are highest in the proximal domain and elevated near the lateral rim (Fig. S7A). K_{PD} is also enhanced on the abaxial (B) surface of the canvas to promote slight curvature towards the apex, promoted slightly distally to keep the tip straight, and inhibited at the edge of the PZ margin.

$\mathbf{K_{PDA}} = m_{BLADE}\ \mathbf{i_{BLADE}}$

*pro (p_{sPROX}, ($\mathbf{s_{PROX}} > t_{sPROX}$) * inh ($h_{sPROX}$, ($\mathbf{s_{PROX}}$- n_1)^2) * ($m_{CENTRAL}\ \mathbf{i_{CENTRAL}}$ + $m_{LATERAL}\ \mathbf{i_{LATERAL}}$ + $m_{MARGINAL}\ \mathbf{i_{MARGINAL}}$) * inh ($h_{sMID}$, ($1$ - $\mathbf{s_{MID}}$)))

*inh ($h_{PZMARGIN}$, $\mathbf{s_{PZMARGIN}}$)

*pro ($p_{sTIP.sMID}$, ($\mathbf{s_{TIP}} > t_{sTIP}$) * ($1$ - $\mathbf{s_{MID}}$))

*inh (h_{sPROXB}, ($\mathbf{s_{PROX}} < t_{sPROX}$))

*inh ($h_{sMARGINAL}$, $\mathbf{s_{MARGINAL}}$)

*inh ($h_{PZMARGIN.MARGINAL}$, $\mathbf{i_{PZMARGIN}} * \mathbf{i_{MARGINAL}}$)

$\mathbf{K_{PDB}} = \mathbf{K_{PDA}} + n_2$

$\mathbf{K_{PERB}} = m_{BLADE}\ \mathbf{i_{BLADE}}$

*inh (h_{sMID}, $\mathbf{s_{MID}}$)

*inh (h_{MID}, $\mathbf{i_{MID}}$)

*inh (h_{sTIP}, $\mathbf{s_{TIP}}$)

*pro (p_{sRIM}, (**sRIM** > t_{sRIM}) * inh ($h_{sPZMARGIN}$, **sPZMARGIN**) * inh ($h_{sMARGINAL}$, **sMARGINAL**)

*inh (h_{sMIDB}, **sMID**) * inh ($h_{PZMARGIN.MARGINAL}$, **iPZMARGIN** * **iMARGINAL**))

K$_{PERA}$ = **K**$_{PERB}$

K$_{NOR}$ = *nbase*

PHASE 1 Petiole-Sheath Hypothesis Model (Fig.4L-M, Fig.S5A-B)

Primordium emerges from the ring. A mediolateral gradient in K_{PD} promotes growth in proximal regions to drive primordium emergence, similar to grass model phase 1. K_{PD} also promoted in the lateral rim to prevent the primordium bending excessively over the apex. K_{PER} is reduced near the midline and promoted by RIM, causing the lateral rim to become more vertical, similar to phases 1 and 2 of the grass model. (Fig.S5A-B). Resultant areal growth rates are thus highest in the proximal domain and elevated near the lateral rim (Fig. S7C). K_{PD} is also promoted slightly in the lateral rim to keep the tip straight as in the grass model.

K$_{PDA}$ = m_{BLADE} **iBLADE**

*pro (p_{sPROX}, (**sPROX**> t_{sPROX}) * inh (h_{sPROX}, (**sPROX**- n_1)^2)

* (**iCENTRAL** + $m_{LATERAL.sMID}$ **iLATERAL** * **sMID**))

*inh (h_{sMID}, (*1* - **sMID**))

*pro ($p_{sPROX.sRIM.sMID.LATERAL}$, (**sPROX** <= t_{sPROX}) * **sRIM** * (**sMID** > t_{sMID}) * **iLATERAL**)

*inh ($h_{MARGINAL}$, **iMARGINAL**)

K$_{PDB}$ = **K**$_{PDA}$

K$_{PERB}$ = m_{BLADE} **iBLADE**

*inh ($h_{sMID.CENTRAL}$, **sMID** * **iCENTRAL**)

*inh (h_{MID}, **iMID**)

*inh (h_{sTIP}, **sTIP**)

906 *pro (p_{sRIM}, ($\mathbf{s_{RIM}} > t_{sRIM}$) * ($\mathbf{i_{CENTRAL}} + \mathbf{i_{LATERAL}}$))

907 $\mathbf{K_{PERA}} = \mathbf{K_{PERB}}$

908 $\mathbf{K_{NOR}} = nbase$

909

910 **PHASE 1 Petiole-Leaf Hypothesis Model (Fig.4P-Q, Fig.S6A-D)**

911 Primordium emerges from the ring. Same as the petiole-sheath model phase 1 until
912 timestep 0.7, when the distal upper leaf (DUL), proximal upper leaf (PUL) and lower
913 leaf (LL) domains are introduced (Fig.4P). After this point, K_{PD} is promoted in the
914 medial distal regions of LL and in the lateral regions of UL, and DUL promotes K_{PER}
915 .(Fig.6C-D). After timestep 0.7 the KRN is:

916 $\mathbf{K_{PDA}} = m_{BLADE}\ \mathbf{i_{BLADE}}$

917 *pro (p_{sPROX}, ($\mathbf{s_{PROX}} > t_{sPROX}$) * inh ($h_{sPROX}$, ($\mathbf{s_{PROX}}$- n_1)^2)

918 * ($\mathbf{i_{CENTRAL}} + m_{LATERAL.sMID} * \mathbf{i_{LATERAL}} * \mathbf{s_{MID}}$) * $\mathbf{i_{UL}}$)

919 *inh ($h_{MARGINAL}$, $\mathbf{i_{MARGINAL}}$)

920 *pro ($p_{sPROX.LL.sSTBOUND}$, ($\mathbf{s_{PROX}} <= t_{sPROX}$) * $\mathbf{i_{LL}}$* inh($h_{sSTBOUND}$, $\mathbf{s_{STBOUND}} > t_{STBOUND}$))

921 *pro (p_{UL}, $\mathbf{i_{UL}}$ * inh ($h_{CENTRAL}$, $\mathbf{i_{CENTRAL}}$))

922 $\mathbf{K_{PDB}} = \mathbf{K_{PDA}}$

923 $\mathbf{K_{PERB}} = m_{BLADE}\ \mathbf{i_{BLADE}}$

924 *inh ($h_{sMID.CENTRAL}$, $\mathbf{s_{MID}} * \mathbf{i_{CENTRAL}}$) * ($\mathbf{i_{LL}}$)

925 *inh (h_{MID}, $\mathbf{i_{MID}}$ * ($\mathbf{i_{LL}}$))

926 *inh (h_{sTIP}, $\mathbf{s_{TIP}}$ * ($\mathbf{i_{LL}}$))

927 *pro (p_{sRIM}, ($\mathbf{s_{RIM}} > t_{sRIM}$) * ($\mathbf{i_{CENTRAL}} + \mathbf{i_{LATERAL}}$))

928 *pro (p_{DUL}, $\mathbf{i_{DUL}}$* pro ($p_{sTIP.MID}$, $\mathbf{s_{TIP}}$ * ($\mathbf{i_{MID}} < t$))

929 *inh ($h_{CENTRAL.sTIP}$, $\mathbf{i_{CENTRAL}}$ * ($\mathbf{s_{TIP}} < t_{sTIP}$)))

930 $\mathbf{K_{PERA}} = \mathbf{K_{PERB}}$

$\mathbf{K_{NOR}} = nbase$

PHASE 2 Grass Model (Fig.3E-G, Fig.S4C-D)

From P2 to P4, when the edges of the primordium overlap. As with phase 1, K_{PD} is promoted in a proximal domain with rates declining along the mediolateral (central-marginal) axis (Fig.S4C), and K_{PER} is promoted in a complementary pattern by RIM and inhibited towards the limits of the central and marginal domains (Fig.S4D). Thus, resultant areal growth rates are highest in the lateral rim and elevated proximally (Fig. S7A). K_{PD} is also promoted slightly in the rim except for in the WRAPPER domain to reduce shape asymmetries caused by the overlapping ends, and inhibited at the edge of the PZ margin.

$\mathbf{K_{PDA}} = m_{BLADE}\ \mathbf{i_{BLADE}}$

*pro (p_{sPROX}, ($\mathbf{s_{PROX}} > t_{sPROX}$) * inh ($h_{sPROX}$, ($\mathbf{s_{PROX}}$ - n_1)^2)

* ($\mathbf{i_{CENTRAL}}$ + ($m_{LATERAL}\ \mathbf{i_{LATERAL}} + m_{MARGINAL}\ \mathbf{i_{MARGINAL}}$) * $\mathbf{s_{MID}}$))

*inh ($h_{sPZMARGIN.sRIM}$, ($\mathbf{s_{PZMARGIN}} > t_{sPZMARGIN}$) * ($\mathbf{s_{RIM}} > t_{sRIM}$))

*pro ($p_{sMARGINAL.sRIM}$, ($\mathbf{s_{MARGINAL}} > t_{sMARGINAL}$) * ($\mathbf{s_{RIM}} > t_{sRIM}$))

*pro (p_{sPROXB}, ($\mathbf{s_{PROX}} > t_{sPROX}$) * $\mathbf{s_{PROX}}$)

*pro ($p_{sMARGINAL.sRIM.WRAPPER}$, ($\mathbf{s_{MARGINAL}} > t_{sMARGINALB}$) * ($\mathbf{s_{RIM}} > t_{sRIM}$)

* ($\mathbf{i_{WRAPPER}} < t$))

*inh ($h_{sRIM.sPROX.sTIP}$, ($\mathbf{s_{RIM}} > t_{sRIMB}$) * ($1$- $\mathbf{s_{PROX}}$) * ($\mathbf{s_{TIP}} > t_{sTIP}$)

*inh ($h_{PZMARGIN.MARGINAL}$, ($\mathbf{i_{PZMARGIN}}$ * $\mathbf{i_{MARGINAL}}$))

*inh ($h_{sTIP.sMID}$, ($\mathbf{s_{TIP}} > t_{sTIP}$) * ($\mathbf{s_{MID}} > t_{sMID}$))

$\mathbf{K_{PDB}} = \mathbf{K_{PDA}}$

$\mathbf{K_{PERB}} = m_{BLADE}\ \mathbf{i_{BLADE}}$

*inh ($h_{sMID+MID}$, ($\mathbf{s_{MID}} + \mathbf{i_{MID}}$))

*pro (p_{sRIM}, ($\mathbf{s_{RIM}} > t_{sRIM}$) * inh ($h_{sTIP}$, $\mathbf{s_{TIP}}$) * ($\mathbf{s_{TIP}} > t_{sTIP}$)

*inh ($h_{sPZMARGIN}$, $\mathbf{s_{PZMARGIN}}$) * pro ($p_{sMARGINAL}$, $\mathbf{s_{MARGINAL}}$)

*inh ($h_{sMARGINAL}$, ($\mathbf{s_{MARGINAL}} > t_{sMARGINAL}$) * $\mathbf{s_{MARGINAL}}$)

*inh ($h_{PZMARGIN.MARGINAL}$, $\mathbf{i_{PZMARGIN}} * \mathbf{i_{MARGINAL}}$))

$\mathbf{K_{PERA}} = \mathbf{K_{PERB}}$

$\mathbf{K_{NOR}} = nbase$

PHASE 2 Petiole-Sheath Hypothesis Model (Fig.4M-N, Fig.S5C-D)

Primordium elongates and broadens. As for phase 1 of the petiole-sheath model, K_{PD} is promoted in a proximal domain with rates declining along the mediolateral (central-marginal) axis (Fig.S5C). This proximal domain is located above the ring of insertion in the stem to reduce excessive growth conflicts at the boundary between primordium and stem. K_{PER} is promoted distal to this domain (Fig.S5D). Resultant areal growth rates are thus highest proximally (Fig. S7C). K_{PER} is promoted in the stipules to drive stipule outgrowth (Fig.S5D), and on the adaxial surface (A-side) to promote lamina flattening.

$\mathbf{K_{PDA}} = m_{BLADE}\ \mathbf{i_{BLADE}}$

*pro ($p_{sLEAFBASE}$, ($\mathbf{s_{LEAFBASE}} < t_{sLEAFBASE}$) * ($\mathbf{i_{CENTRAL}} + \mathbf{i_{LATERAL}}$) * inh ($h_{sMID}$, $\mathbf{s_{MID}}$))

*inh ($h_{LEAFBASE}$, $\mathbf{i_{LEAFBASE}}$)

*inh ($h_{MARGINAL}$, $\mathbf{i_{MARGINAL}}$)

*inh ($h_{sLEAFBASE.sTIP}$, ($\mathbf{s_{LEAFBASE}} < t_{sLEAFBASE}$) * $\mathbf{s_{TIP}}$)

*inh ($h_{STBOUND}$, $\mathbf{i_{STBOUND}}$)

$\mathbf{K_{PDB}} = \mathbf{K_{PDA}}$

$\mathbf{K_{PERB}} = m_{BLADE}\ \mathbf{i_{BLADE}}$

*pro ($p_{STIPULE.sRIM.sSTBOUND}$, $\mathbf{i_{STIPULE}} * (\mathbf{s_{RIM}} > t_{sRIM}) * (\mathbf{s_{STBOUND}} > t_{sSTBOUND})$)

*inh ($h_{sSTBOUND}$, $\mathbf{s_{STBOUND}}$)

$\mathbf{K_{PERA}} = \mathbf{K_{PERB}}$

+ ($\mathbf{i_{CENTRAL}} + \mathbf{i_{LATERAL}}$) * (*1*- $\mathbf{s_{TIP}}$) * ($\mathbf{s_{LEAFBASE}} < t_{sLEAFBASE}$)

$\mathbf{K_{NOR}} = nbase$

PHASE 2 Petiole-Leaf Hypothesis Model (Fig.4Q-R, Fig.S6C-D)

Primordium elongates and broadens. K_{PD} promoted by DUL to promote growth of the lamina (Fig.S6C). K_{PER} is similarly promoted by DUL except the midline region (Fig.S6D). Resultant areal growth rates are thus highest in the DUL domain (Fig. S7E). K_{PER} is promoted in the stipules to drive stipule outgrowth (Fig.S6D).

$\mathbf{K_{PDA}} = m_{BLADE}\ \mathbf{i_{BLADE}}$

*inh ($h_{LEAFBASE}$, $\mathbf{i_{LEAFBASE}}$)

*inh ($h_{MARGINAL}$, $\mathbf{i_{MARGINAL}}$)

*inh ($h_{STBOUND}$, $\mathbf{i_{STBOUND}}$)

*pro (p_{DUL}, $\mathbf{i_{DUL}}$ * inh ($h_{STIPULE}$, $\mathbf{i_{STIPULE}}$))

*inh (h_{LL+PUL}, ($\mathbf{i_{LL}} + \mathbf{i_{PUL}}$))

*inh (h_{sTIP}, $\mathbf{s_{TIP}}$)

$\mathbf{K_{PDB}} = \mathbf{K_{PDA}}$

$\mathbf{K_{PERB}} = m_{BLADE}\ \mathbf{i_{BLADE}}$

*pro ($p_{STIPULE.sRIM.sSTBOUND}$, $\mathbf{i_{STIPULE}}$ * ($\mathbf{s_{RIM}} > t_{sRIM}$) * ($\mathbf{s_{STBOUND}} > t_{sSTBOUND}$))

*inh ($h_{sSTBOUND}$, $\mathbf{s_{STBOUND}}$)

*inh ($h_{sMID+MID}$, $\mathbf{s_{MID}} + \mathbf{i_{MID}}$)

*inh ($h_{LL.CENTRAL+LATERAL}$, $\mathbf{i_{LL}}$ * ($\mathbf{i_{CENTRAL}} + \mathbf{i_{LATERAL}}$))

pro ($p_{DUL.sMID}$, $\mathbf{i_{DUL}}$ ($\mathbf{s_{MID}} > t_{sMID}$))

$\mathbf{K_{PERA}} = \mathbf{K_{PERB}}$

$\mathbf{K_{NOR}} = nbase$

PHASE 3 Grass Model (Fig.3G-H, Fig.S4E-F)

Sheath domain is established and leaf grows from base. K_{PD} is promoted at the base of the SHEATH and base of the BLADE, and slightly at the tip to promote blade opening (Fig.S4E). K_{PD} is also inhibited at the edge of the PZ margin, and in the ring of insertion in the stem to reduce excessive growth conflicts at the boundary between primordium and stem. K_{PER} is promoted by BLADE (Fig.S4F). Resultant growth rates are highest in the leaf base (Fig. S7A).

$\mathbf{K_{PDA}} = m_{PZ}\ \mathbf{i_{PZ}}$

*inh ($h_{LEAFBASE}$, $\mathbf{i_{LEAFBASE}}$)

*pro (p_{SHEATH}, $\mathbf{i_{SHEATH}} * (\mathbf{s_{LEAFBASE}} > t_{sLEAFBASE})$)

*pro ($p_{BLADE.sPROX2}$, $\mathbf{i_{BLADE}} * (\mathbf{s_{PROX2}} > t_{sPROX2}) * (\mathbf{s_{PROX2}} < t_{sPROX2B})$

*pro ($p_{sMARGINAL.sRIM}$, $\mathbf{s_{MARGINAL}} * (\mathbf{s_{RIM}} > t_{sRIM}) * \mathbf{s_{RIM}}$))

*pro ($p_{BLADE.sTIP.sPROX2.sRIM}$, $\mathbf{i_{BLADE}} * (\mathbf{s_{TIP}} > t_{sTIP}) * (\mathbf{s_{PROX2}} > t_{sPROX2}) * \mathbf{s_{RIM}}$

*inh (h_{sMID}, $\mathbf{s_{MID}}$)

*inh ($h_{sTIP.sPROX2}$, $(\mathbf{s_{TIP}} > t_{sTIPB}) * (\mathbf{s_{PROX2}} > t_{sPROX2})$)

*inh ($h_{PZMARGIN.MARGINAL}$, $\mathbf{i_{PZMARGIN}} * \mathbf{i_{MARGINAL}}$)

$\mathbf{K_{PDB}} = \mathbf{K_{PDA}}$

$\mathbf{K_{PERB}} = m_{PZ}\ \mathbf{i_{PZ}}$

* pro ($p_{BLADE.sPROX2.sRIM}$, $\mathbf{i_{BLADE}} * \mathbf{s_{PROX2}} * (\mathbf{s_{RIM}} > t_{sRIM})$)

$\mathbf{K_{PERA}} = \mathbf{K_{PERB}}$

$+ m_{BLADE}\ \mathbf{i_{BLADE}}$

$\mathbf{K_{NOR}} = nbase$

PHASE 3 Petiole-Sheath Hypothesis Model (Fig.4N-O, Fig.S5E-F)

Extension of petiole and widening of lamina. At the start of this stage, polarity reorients in the stipules towards their tips. K_{PD} is promoted by SHEATH (petiole), proximally in BLADE (lamina) and by STIPULE, and inhibited at the stipule-lamina boundary (Fig.S5E). K_{PER} is promoted in proximal non-midvein regions of the lateral blade, enhanced by OLATERAL, broadening the lamina (Fig.S5F), similar to the grass model during phase 2 (Fig.S4D). Resultant growth rates are highest in the proximal non-midvein region of the lateral lamina (Fig. S7C). K_{PD} is also inhibited in the abaxial (B-side) of the stipules to promote their outward bending.

$\mathbf{K_{PDA}} = m_{PZ}\ \mathbf{i_{PZ}}$

*pro (p_{SHEATH}, $\mathbf{i_{SHEATH}}$)

*pro ($p_{BLADE.sPROX2}$, $\mathbf{i_{BLADE}}$ * $\mathbf{s_{PROX2}}$ * pro (p_{sRIM}, ($\mathbf{s_{RIM}} > t_{sRIM}$)))

*inh (h_{sTIP}, $\mathbf{s_{TIP}}$)

*inh (h_{sMID}, $\mathbf{s_{MID}}$)

*inh ($h_{sLEAFBASE.sTIP}$, ($\mathbf{s_{LEAFBASE}} < t_{sLEAFBASE}$))

*pro ($p_{STIPULE.sPROX}$, $\mathbf{i_{STIPULE}}$ * ($\mathbf{s_{PROX}} > t_{sPROX}$))

*inh ($h_{STBOUND}$, $\mathbf{i_{STBOUND}}$)

$\mathbf{K_{PDB}} = \mathbf{K_{PDA}}$

*inh ($h_{STIPULE}$, $\mathbf{i_{STIPULE}}$)

$\mathbf{K_{PERB}} = m_{PZ}\ \mathbf{i_{PZ}}$

*pro ($p_{BLADE.sPROX2.sTIP}$, $\mathbf{i_{BLADE}}$ * ($\mathbf{s_{PROX2}}$ + (*1*- $\mathbf{s_{TIP}}$)) * $\mathbf{i_{LATERAL}}$

*pro ($p_{OLATERAL}$, $\mathbf{i_{OLATERAL}}$) * ($\mathbf{s_{RIM}} > t_{sRIM}$) * pro ($p_{sRIM}$, $\mathbf{s_{RIM}}$) * inh (h_{sTIP}, $\mathbf{s_{TIP}}$)

*pro ($p_{LEAFBASE}$, $\mathbf{i_{LEAFBASE}}$)

$\mathbf{K_{PERA}} = \mathbf{K_{PERB}}$

$\mathbf{K_{NOR}} = nbase$

PHASE 3 Petiole-Leaf Hypothesis Model (Fig.4R-S, Fig.S6E-F)

Extension of petiole and widening of lamina. K_{PD} is promoted by PUL (petiole) and STIPULE, and inhibited at the stipule-lamina boundary (Fig. S6E). K_{PER} is promoted in the non-midvein region of DUL (lamina). Resultant growth rates are highest in the stipules, petiole and non-midvein region of the lamina (Fig. S7E). K_{PD} is also inhibited in the abaxial (B-side) of the stipules to promote their outward bending.

$\mathbf{K_{PDA}} = m_{PZ}\ \mathbf{i_{PZ}}$

*pro ($p_{STIPULE.sPROX}$, $\mathbf{i_{STIPULE}}$ * ($\mathbf{s_{PROX}} > t_{sPROX}$)

*inh ($h_{STBOUND}$, $\mathbf{i_{STBOUND}}$)

pro ($p_{PUL.sPROX2}$, $\mathbf{i_{PUL}}$ ($\mathbf{s_{PROX2}} > t_{sPROX2}$))

$\mathbf{K_{PDB}} = \mathbf{K_{PDA}}$

*inh ($h_{STIPULE}$, $\mathbf{i_{STIPULE}}$)

$\mathbf{K_{PERB}} = m_{PZ}$ * $\mathbf{i_{PZ}}$

*pro (p_{sPROX2}, $\mathbf{s_{PROX2}}$)

*inh ($h_{MID+sMID+sTIP+PUL}$, ($m_{MID}\ \mathbf{i_{MID}} + m_{sMID}\ \mathbf{s_{MID}} + \mathbf{s_{TIP}} + m_{PUL}\ \mathbf{i_{PUL}}$)

*pro ($p_{DUL.sMID}$, $\mathbf{i_{DUL}}$ * ($\mathbf{s_{MID}} > t_{sMID}$))

$\mathbf{K_{PERA}} = \mathbf{K_{PERB}}$

$\mathbf{K_{NOR}} = nbase$

PHASE 4 Grass Model (Fig.3G-H, Fig.S4G-H)

Sheath extends and blade unwraps. K_{PD} is promoted at the base of the SHEATH and base of the BLADE (Fig.S4G). K_{PD} is also inhibited at the edge of the PZ margin, and in the ring of insertion in the stem to reduce excessive growth conflicts at the boundary between primordium and stem. K_{PER} is promoted on adaxial surface (A-side) by in

proximal margin of BLADE to promote blade opening (Fig.S4H). Resultant growth rates are highest in the sheath and blade bases (Fig. S7A).

$\mathbf{K_{PDA}} = m_{PZ}\ \mathbf{i_{PZ}}$

*inh ($h_{LEAFBASE}$, $\mathbf{i_{LEAFBASE}}$)

*pro ($p_{SHEATH.sLEAFBASE}$, $\mathbf{i_{SHEATH}} * (\mathbf{s_{LEAFBASE}} > t_{sLEAFBASE})$)

*pro ($p_{BLADE.sPROX2}$, $\mathbf{i_{BLADE}} * (\mathbf{s_{PROX2}} > t_{sPROX2}) * (\mathbf{s_{PROX2}} < t_{sPROX2B})$ * pro ($p_{sMARGINAL.sRIM}$, $\mathbf{s_{MARGINAL}} * (\mathbf{s_{RIM}} > t_{sRIM}) * \mathbf{s_{RIM}}$))

*inh ($h_{BLADE.sPROX2.sTIP}$, $\mathbf{i_{BLADE}} * (\mathbf{s_{PROX2}} < t_{sPROX2})$ * pro (p_{sTIP}, $(\mathbf{s_{TIP}} > t_{sTIP})$))

*inh ($h_{PZMARGIN.MARGINAL}$, $\mathbf{i_{PZMARGIN}} * \mathbf{i_{MARGINAL}}$)

$\mathbf{K_{PDB}} = \mathbf{K_{PDA}}$

$\mathbf{K_{PERB}} = m_{PZ} * \mathbf{i_{PZ}}$

$\mathbf{K_{PERA}} = \mathbf{K_{PERB}}$

$+ m_{MARGINAL}\ \mathbf{i_{MARGINAL}} * \mathbf{s_{RIM}} * (\mathbf{s_{RIM}} > t_{sRIM}) * (\mathbf{s_{PROX2}} < t_{sPROX2A}) * (\mathbf{s_{PROX2}} > t_{sPROX2B})$

$* \mathbf{i_{BLADE}}$

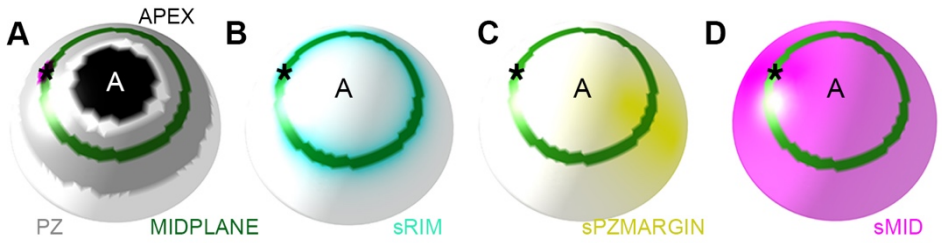

Fig. S1. Additional regional factors in the volumetric primordium emergence models.

(**A-D**) Factors and polarities involved in growth regulatory network, in addition to those in Fig.2. (**A**) PZ (grey) encircles the APEX (black) domain. The boundary between the abaxial and adaxial domains (MIDPLANE, dark green) is within the PZ. The future MIDVENTIP (magenta, *) is centred on MIDPLANE. (**B**) sRIM (cyan) concentration decreases from MIDPLANE toward the PZ edges. (**C**) sPZMARGIN (yellow) increases in concentration towards the position opposite the MIDVEINTIP (*). (D) sMID is highest in the PZ on the side of the MIDVENTIP (*) and decreases mediolaterally.

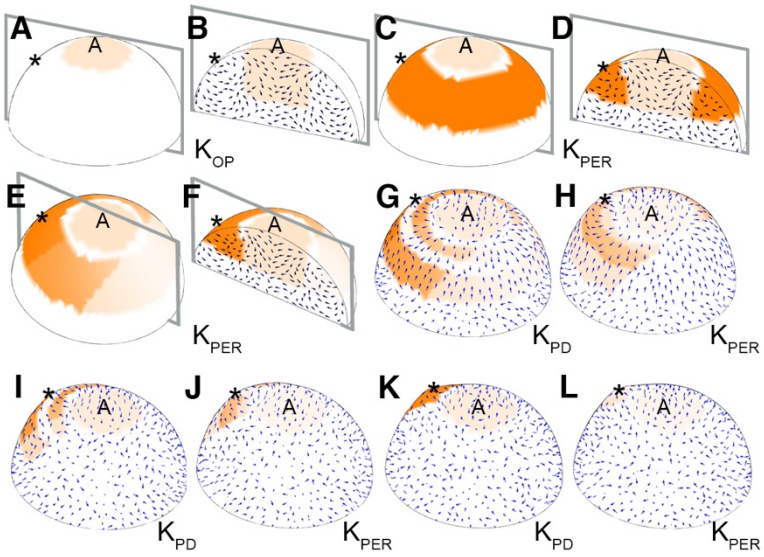

Fig. S2. Specified growth rate patterns in the volumetric primordium emergence models

Specified growth rate (orange) patterns parallel (K_{OP}) (**A-B**) to the orthoplanar polarity field (black arrows), parallel (K_{PD}) (**G,I,K**) to the proximodistal polarity field (blue arrows) and perpendicular to both (K_{PER}) (**C,D,E,F,H,J,L**). All primordium emergence models share the same pattern of K_{OP} (**A-B**). (**C-F**) The initial emergence models with just an orthoplanar polarity field, where growth is specified as: (A-D Fig.2C-D) or (A-B,E-F, Fig.2E-F) growth is modulated mediolaterally. (**G-L**) Emergence models with both orthoplanar and proximodistal polarity fields. (G-H) Wildtype grass leaf (Fig.2I-L), (I-J) Wildtype eudicot primordium emergence model (Fig.4C-D). (K-L) The ad-abaxial mutant (Fig.4F-G). The K_{OP}, K_{PD}, and K_{PER} scale (gradient of orange, white: 0, dark orange: 0.55) is the same for each model. Midvein tip: *. Meristem apex: A.

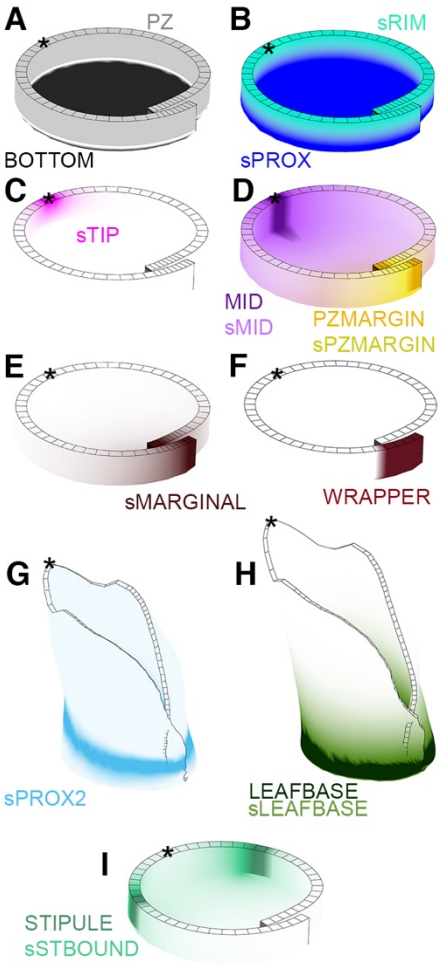

Fig. S3. Regional factors in the tissue sheet models of leaf development.

(**A-G**) Factors involved in the growth regulatory networks, in addition to those shown in Fig.3 and Fig.4. (**A-D**) Are present throughout the models. (**E-F**) Are unique to the grass leaf model. (**G-H**) The factor in G is promoted by SHEATH, introduced at the end of phase 2 in both models. The factors in H are introduced at the start of phase 2 in the eudicot models, and at the end of phase 2 for the grass models. (**I**) Factors unique to the eudicot model. (**A**) The canvas is separated into PZ and BOTTOM domains. (**B**) sRIM (turquoise) increases in concentration towards the rim of the canvas (corresponding to the surface midplane in the volumetric models). sPROX (royal blue) increases in concentration towards the base, complementary to sRIM. (**C**) sTIP (magenta) is produced at the midvein tip, and diffuses outwards. (**D**) sMID

(light purple) increases in concentration towards MID (dark purple). sPZMARGIN (yellow) increases in concentration towards PZMARGIN (orange). (E) sMARGINAL (brown) is restricted to the MARGINAL domain, and increases in concentration towards the PZ margin edges. (**F**) WRAPPER (brown) is on the outer wrapped edge. (**G**) sPROX2 (light blue) is activated at the P4 stage and is highest in the proximal base. (**H**) sLEAFBASE (light green) increases in concentration towards LEAFBASE (dark green). (I) The eudicot model assigns STIPULE identity (dark turquoise) in the MARGINAL domain, and sSTBOUND (light turquoise) is produced at the boundary between MARGINAL and OLATERAL. Midvein tip: asterisk.

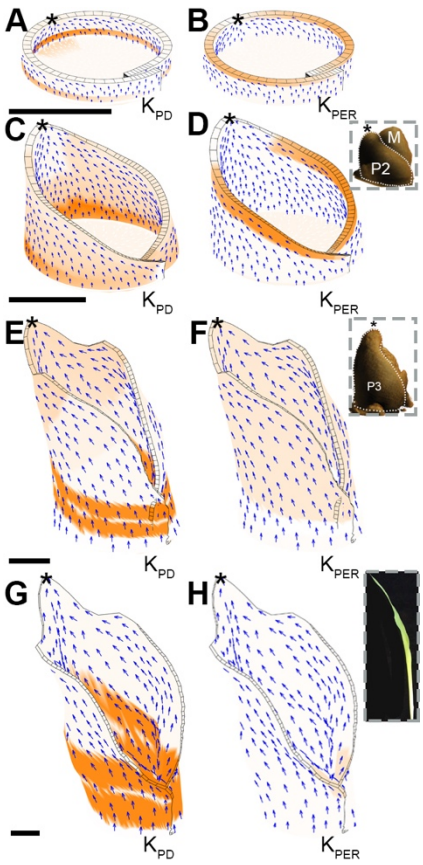

Fig. S4 Specified growth rate patterns in the wildtype grass leaf tissue sheet model

Specified growth rate (orange) patterns parallel (K_{PD}) (A,C,E,G) and perpendicular (K_{PER}) (B,D,F,H) to the proximal-distal polarity field (PD, blue arrows). In phase 1 (A-B), phase 2 (C-D), phase 3 (E-F), and phase 4 (G-H) of the wildtype grass leaf model. K_{PD} and K_{PER} scale (orange) is the same for each phase. Maximal values are listed in Table S4. Insets are representative images of the relative stages. Scalebar is in arbitrary units. Midvein tip: *.

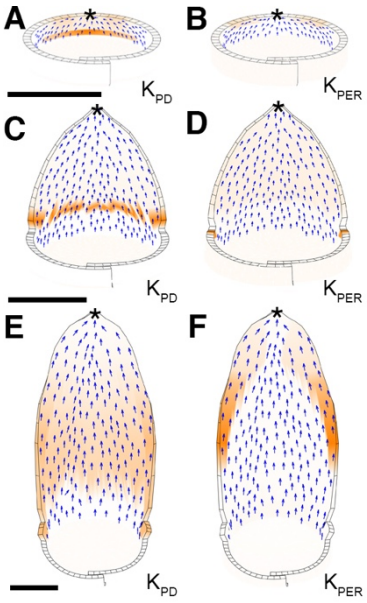

Fig. S5 Specified growth rate patterns in the petiole-sheath hypothesis tissue sheet model

Specified growth rate (orange) patterns parallel (K_{PD}) (A,C,E) and perpendicular (K_{PER}) (B,D,F) to the proximal-distal polarity field (PD, blue arrows). In phase 1 (A-B), phase 2 (C-D), and phase 3 (E-F) of the petiole-sheath hypothesis model. K_{PD} and K_{PER} scale (orange) is the same for each phase. Maximal values are listed in Table S4. Scalebar is in arbitrary units. Midvein tip: *.

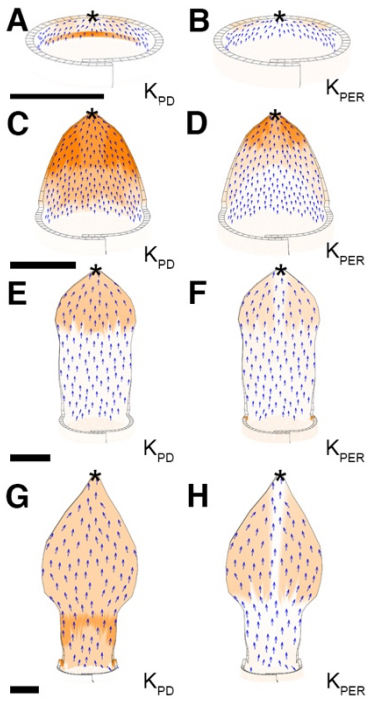

Fig. S6 Specified growth rate patterns in the petiole-leaf hypothesis tissue sheet model

Specified growth rate (orange) patterns parallel (K_{PD}) (A,C,E,G) and perpendicular (K_{PER}) (B,D,F,H) to the proximal-distal polarity field (PD, blue arrows). In phase 1 before timestep 0.7 (A-B), phase 1 after timestep 0.7 (C-D), phase 2 (E-F), and phase 3 (G-H) of the petiole-leaf hypothesis model. K_{PD} and K_{PER} scale (orange) is the same for each phase. Maximal values are listed in Table S4. Scalebar is in arbitrary units. Midvein tip: *.

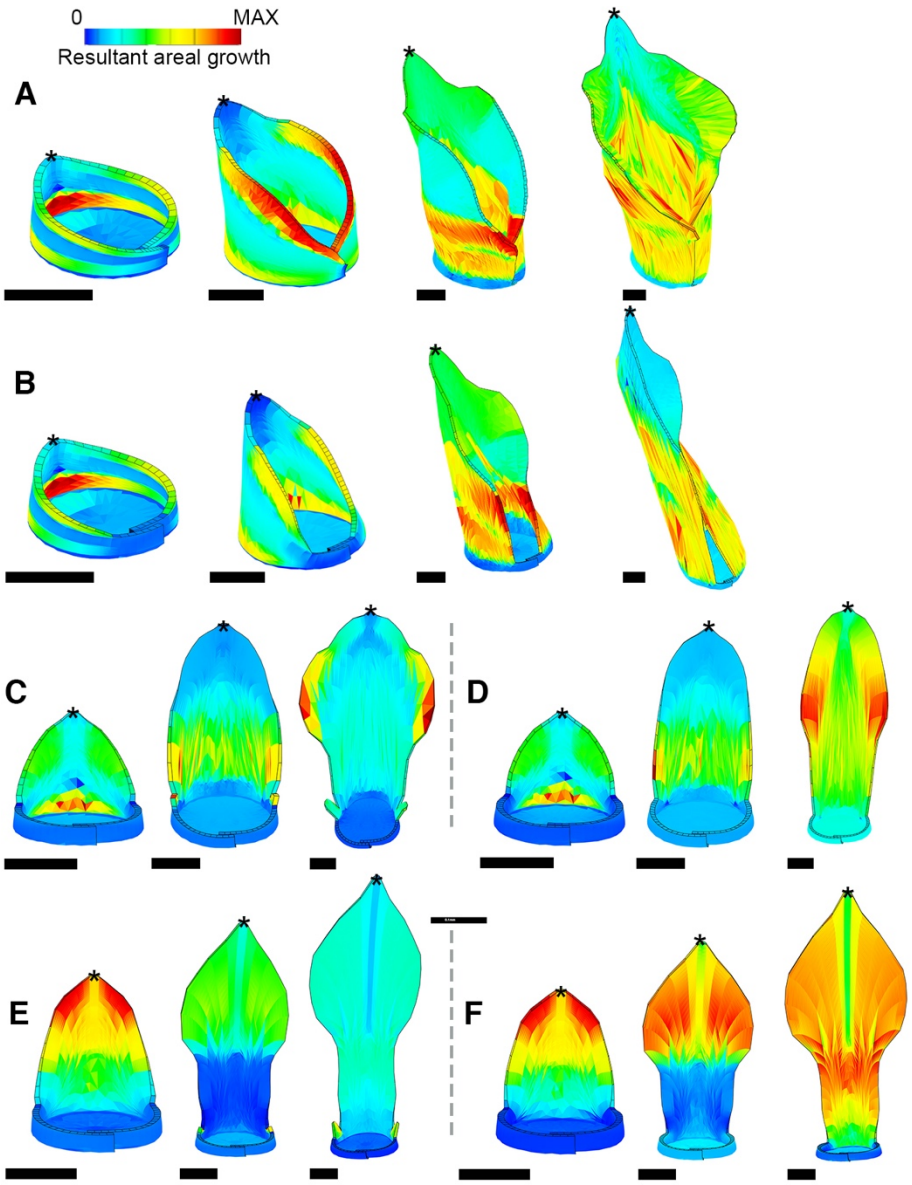

Fig. S7 Resultant areal growth rate patterns in the tissue sheet models

Resultant areal growth rate patterns. Phase 1-4 of the wild-type grass leaf model (A), the *ns* mutant model (B). Phases 1-3 of the petiole-sheath hypothesis model (C), the petiole-sheath *prs/wox1* mutant model (D), the petiole-leaf hypothesis model (E) and the petiole-leaf prs/wox1 mutant model (F). Resultant areal growth rate is shown by the colour gradient, the minimum value is 0 (dark blue) and the maximum value is shown in Table S3 (red). Scale bars are in arbitrary units. Midvein tip: *.

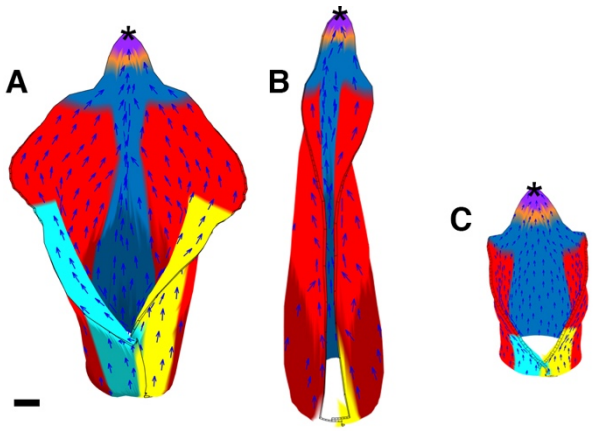

Fig. S8 Final morphology of variations in the grass leaf tissue sheet model. The effect of changing factor effects in the grass leaf tissue sheet model. (**A**) wild-type model. (**B**) *ns* mutant model; removal of the MARGINAL domain. (**C**) *bop* mutant model: removal of the SHEATH domain leading to ectopic BLADE and shortening of the leaf base due to lack of growth-promoting signals from the SHEATH domain. Scale bar is in arbitrary units. Midvein tip (*).

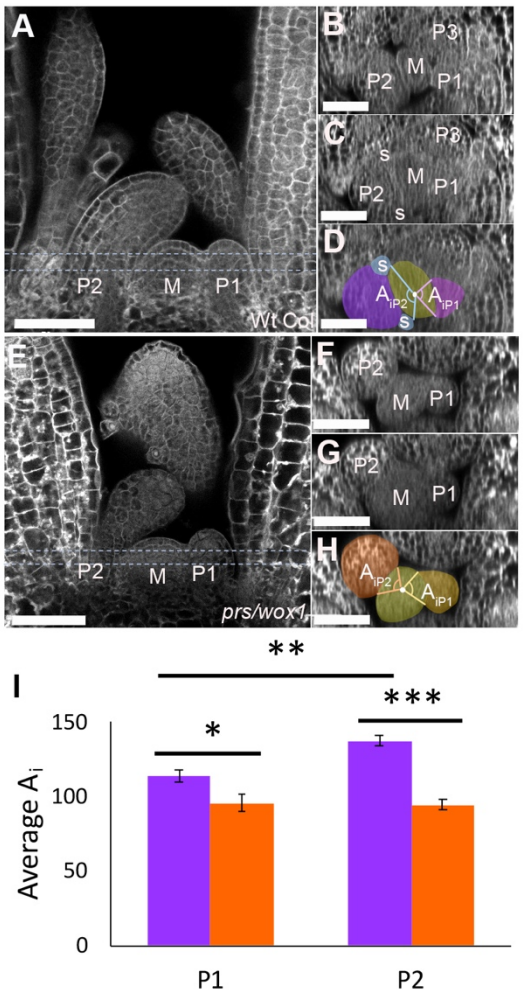

Fig. S9. **Double mutant *prs/wox1* leaves are narrower than wild type leaves at their initial emergence from the shoot apical meristem (SAM).**

(A-H) Confocal images of propidium iodide (PI) stained WT Col (A-D) and *prs/wox1* double mutant (E-H) SAMs and young leaf primordia. (A,E) Longitudinal (XY) section through the SAM, P1, and P2 representing the longitudinal z-stack collected through the SAM and early leaf primordia for WT Col and *prs wox1*, respectively. Dashed lines mark optical orthogonal sections in the transverse (ZX) plane of the P1 attachment point (B,F) and of the P2 attachment point (C,G) for WT Col and *prs wox1* samples, respectively. (D,H) Outlines of SAM, P1, and P2 overlaid on optical transverse sections of WT Col and *prs wox1* double mutant seedlings, respectively, depicting examples of angle of insertion (A_i) measurements collected on multiple slices traveling

down the SAM until outlines became undiscernible for each biological sample. Note the WT A_i measurements for P2 include the stipules, marked with “s”. (I) Average A_i, computed from the last 5 angle measurements collected for WT col (purple) was significantly larger than for *prs wox1* (orange) as early as the P1 stage; this difference in A_i increases at the P2 stage. The A_i for *prs wox1* mutants remains constant from P1 to P2. WT n_{P1} = 19, n_{P2} = 16; *prs wox1* n_{P1} = 14, n_{P2} = 13. * = 0.014, ** = 0.00052, *** = 7.9×10^{-9}. m = shoot apical meristem, P1 = plastochron 1-staged leaf primordium, P2 = plastochron 2-staged leaf primordium, s = stipule, scale bar = 50 μm, A_{iP1} = angle of insertion for P1, A_{iP2} = angle of insertion for P2.

Parameter	Description	Model Values		
		Ring	Mediolateral	Leaf
K_{OP}				
m_{APEX}	Multiplication of i_{APEX}	0.08	0.08	0.08
K_{PD}				
n_1	Parameter 1	-	-	0.1
$h_{sPZMARGIN}$	Inhibition by $s_{PZMARGIN}$	-	5	5
m_{APEX}	Multiplication of i_{APEX}	0.08	0.08	0.08
$m_{CENTRAL}$	Multiplication of $i_{CENTRAL}$	-	0.4	0.4
$m_{LATERAL}$	Multiplication of $i_{LATERAL}$	-	0.32	0.32
$m_{MARGINAL}$	Multiplication of $i_{MARGINAL}$	-	0.12	0.12
m_{PZ}	Multiplication of i_{PZ}	0.4	-	-
$p_{ABAXIAL}$	Promotion by $i_{ABAXIAL}$	-	-	0.3
p_{sMID}	Promotion by s_{MID}	-	-	-
t_{sRIM}	Threshold of s_{RIM}	-	-	0.7
K_{PER}				
h_{sMID}	Inhibition by s_{MID}	-	-	1
$h_{sPZMARGIN}$	Inhibition by $s_{PZMARGIN}$	-	-	5
h_{sTIP}	Inhibition by s_{TIP}	-	-	0.5
m_{APEX}	Multiplication of i_{APEX}	-	-	0.04
$m_{CENTRAL.PZ}$	Multiplication of $i_{CENTRAL}$	-	-	0.1
$m_{LATERAL.PZ}$	Multiplication of $i_{LATERAL}$	-	-	0.1
$p_{ABAXIAL}$	Promotion by $i_{ABAXIAL}$	-	-	0.3
p_{sMID}	Promotion by s_{MID}	-	-	2
t_{sMID}	Threshold of s_{MID}	-	-	0.95
t_{sRIM}	Threshold of s_{RIM}	-	-	0.5

Table S1. Parameters for the 3D Primordium Emergence Models

Parameters relating to the model code in “Supplementary Text: Model Descriptions”, for all of the Primordium Emergence Models. Parameters are denoted by m_x, p_x, h_x, or n_i, where X defines the factor the parameter relates to, m defines multiplication, p defines promotion and h defines inhibition, and n_i defines additional general parameters. Model “Ring” refers to the Ring Primordium model shown in Fig. 2C,D and Fig.S2A-D. Model “Mediolateral” refers to the model with growth modulated by the mediolateral patterning shown in Fig.2E,F and Fig.S2E-F. “Leaf” refers to both the

grass leaf primordium models shown in Fig.2I-L,P-Q and Fig.S2G-H, and eudicot leaf primordium models shown in Fig.4C-K and Fig.S2I-L.

Parameter	Description	Values WT Grass	Petiole - sheath	Petiole - leaf
K_{NOR} All growth phases				
nbase	Basal growth rate in thickness	0.3	0.3	0.3
K_{PD} Growth Phase 1				
n_1	Parameter 1	0.5	0.5	0.5
n_2	Parameter 4	0.2	-	-
$h_{CENTRAL}$	Inhibition by $i_{CENTRAL}$	-	-	0.3
$h_{MARGINAL}$	Inhibition by $i_{MARGINAL}$	-	100	100
$h_{PZMARGIN.MARGINAL}$	Inhibition by $i_{PZMARGIN}$ multiplied by $i_{MARGINAL}$	100	-	-
$h_{sMARGINAL}$	Inhibition by $s_{MARGINAL}$	2	-	-
h_{sMID}	Inhibition by s_{MID}	0.5	1	-
h_{sPROX}	Inhibition by s_{PROX}	2	2	2
h_{sPROXB}	Inhibition by s_{PROX}	1.5	-	-
$h_{sPZMARGIN}$	Inhibition by $s_{PZMARGIN}$	4	-	-
$h_{sSTBOUND}$	Inhibition by $s_{STBOUND}$	-	-	2
m_{BLADE}	Multiplication of i_{BLADE}	2	2	2
$m_{CENTRAL}$	Multiplication of $i_{CENTRAL}$	0.93	-	-
$m_{LATERAL}$	Multiplication of $i_{LATERAL}$	0.7	-	-
$m_{LATERAL.sMID}$	Multiplication of $i_{LATERAL}$ multiplied by s_{MID}	-	1.2	1.2
$m_{MARGINAL}$	Multiplication of $i_{MARGINAL}$	0.7	-	-
p_{UL}	Promotion by i_{UL}	-	-	7
p_{sPROX}	Promotion by s_{PROX}	5	6	6
$p_{sPROX.LL.sSTBOUND}$	Promotion by s_{PROX} multiplied by i_{LL} and $s_{STBOUND}$	-	-	3
$p_{sPROX.sRIM.sMID.LATERAL}$	Promotion by s_{PROX} multiplied by s_{RIM} and s_{MID} and $i_{LATERAL}$	-	1.5	-
$p_{sTIP.sMID}$	Promotion by s_{TIP} multiplied by s_{MID}	5	-	-
t_{sMID}	Threshold of s_{MID}	-	0.5	0.5
t_{sPROX}	Threshold of s_{PROX}	0.5	0.5	-
$t_{sSTBOUND}$	Threshold of $s_{STBOUND}$	-	-	0.4
t_{sTIP}	Threshold of s_{TIP}	0.2	-	-
K_{PD} Growth Phase 2				
n_1	Parameter 1	0.5	-	-
$h_{LEAFBASE}$	Inhibition by $i_{LEAFBASE}$	-	100	100
h_{LL+PUL}	Inhibition by i_{LL} plus i_{PUL}	-	-	100
$h_{MARGINAL}$	Inhibition by $i_{MARGINAL}$	-	100	100
$h_{STBOUND}$	Inhibition by $i_{STBOUND}$	-	100	100
$h_{STIPULE}$	Inhibition by $i_{STIPULE}$	-	-	5
$h_{sLEAFBASE.sTIP}$	Inhibition by $s_{LEAFBASE}$ multiplied by s_{TIP}	-	10	-
$h_{sMARGINAL.sRIM}$	Inhibition by $s_{MARGINAL}$ multiplied by s_{RIM}	1	-	-

h_{sMID}	Inhibition by s_{MID}	-	0.5	-
h_{sPROX}	Inhibition by s_{PROX}	2	-	-
$h_{PZMARGIN.MARGINAL}$	Inhibition by $i_{PZMARGIN}$ multiplied by $i_{MARGINAL}$	100	-	-
$h_{sPZMARGIN.sRIM}$	Inhibition by $s_{PZMARGIN}$ multiplied by s_{RIM}	2	-	-
$h_{sRIM.sPROX.sTIP}$	Inhibition by s_{RIM} multiplied by s_{PROX} and s_{TIP}	0.4	-	-
h_{sTIP}	Inhibition by s_{TIP}	-	-	1
$h_{sTIP.sMID}$	Inhibition by s_{TIP} multiplied by s_{MID}	3	-	-
p_{DUL}	Promotion by i_{DUL}	-	-	1.5
$p_{sLEAFBASE}$	Promotion by $s_{LEAFBASE}$	-	6	-
$p_{sMARGINAL.sRIM.WRAPPER}$	Promotion by $s_{MARGINAL}$ multiplied by s_{RIM} and $i_{WRAPPER}$	0.5	-	-
p_{sPROX}	Promotion by s_{PROX}	5.3	-	-
p_{sPROXB}	Promotion by s_{PROX}	3	-	-
m_{BLADE}	Multiplication of i_{BLADE}	2	2	2
$m_{LATERAL}$	Multiplication of $i_{LATERAL}$	2	-	-
$m_{MARGINAL}$	Multiplication of $i_{MARGINAL}$	2	-	-
t	Threshold of identity factor	0.1	-	-
$t_{sLEAFBASE}$	Threshold of $s_{LEAFBASE}$	-	0.7	-
t_{sMID}	Threshold of s_{MID}	0.8	-	-
$t_{sMARGINAL}$	Threshold of $s_{MARGINAL}$	0.6	-	-
$t_{sMARGINALB}$	Threshold of $s_{MARGINAL}$	0.4	-	-
t_{sPROX}	Threshold of s_{PROX}	0.5	-	-
$t_{sPZMARGIN}$	Threshold of $s_{PZMARGIN}$	0.6	-	-
t_{sRIM}	Threshold of s_{RIM}	0.7	-	-
t_{sRIMB}	Threshold of s_{RIM}	0.8	-	-
t_{sTIP}	Threshold of s_{TIP}	0.2	0.5	-
K_{PD} Growth Phase 3				
$h_{LEAFBASE}$	Inhibition by $i_{LEAFBASE}$	20	-	-
$h_{PZMARGIN.MARGINAL}$	Inhibition by $i_{PZMARGIN}$ multiplied by $i_{MARGINAL}$	100	-	-
$h_{STBOUND}$	Inhibition by $i_{STBOUND}$	-	100	100
$h_{STIPULE}$	Inhibition by $i_{STIPULE}$	-	1	1
$h_{sLEAFBASE.sTIP}$	Inhibition by $s_{LEAFBASE}$ multiplied by s_{TIP}	-	10	-
h_{sMID}	Inhibition by s_{MID}	1	0.5	0.5
h_{sTIP}	Inhibition by s_{TIP}	-	3	-
$h_{sTIP.sPROX2}$	Inhibition by s_{TIP} multiplied by s_{PROX2}	1	-	-
m_{PZ}	Multiplication of i_{PZ}	2	2	2
$p_{BLADE.sPROX2}$	Promotion by i_{BLADE} multiplied by s_{PROX2}	8	5	-
$p_{BLADE.sTIP.sPROX2.sRIM}$	Promotion by i_{BLADE} multiplied by s_{TIP} , s_{PROX2} and s_{RIM}	3	-	-
$p_{PUL.sPROX2}$	Promotion by i_{PUL} multiplied by s_{PROX2}	-	-	1

p_{SHEATH}	Promotion by i_{SHEATH}	8	5	-
$p_{STIPULE.sPROX}$	Promotion by $i_{STIPULE}$ multiplied by s_{PROX}	-	5	5
$p_{sMARGINAL.sRIM}$	Promotion by $s_{MARGINAL}$ multiplied by s_{RIM}	0.5	-	-
p_{sRIM}	Promotion by s_{RIM}	-	0.7	-
$t_{sLEAFBASE}$	Threshold of $s_{LEAFBASE}$	0.5	0.9	-
t_{sPROX}	Threshold of s_{PROX}	-	0.3	0.3
t_{sPROX2}	Threshold of s_{PROX2}	0.5	-	0.1
$t_{sPROX2B}$	Threshold of s_{PROX2}	0.9	-	-
t_{sRIM}	Threshold of s_{RIM}	0.8	0.95	-
t_{sTIP}	Threshold of s_{TIP}	0.1	-	-
t_{sTIPB}	Threshold of s_{TIP}	0.05	-	-
K_{PD} Growth Phase 4				
$h_{BLADE.sPROX2.sTIP}$	Inhibition by i_{BLADE} multiplied by s_{PROX2} and s_{TIP}	1	-	-
$h_{LEAFBASE}$	Inhibition by $i_{LEAFBASE}$	20	-	-
$h_{sPZMARGIN.MARGINAL}$	Inhibition by $s_{PZMARGIN}$ multiplied by $i_{MARGINAL}$	100	-	-
m_{PZ}	Multiplication of i_{PZ}	4	-	-
$p_{BLADE.sPROX2}$	Promotion by i_{BLADE} multiplied by s_{PROX2}	8	-	-
$p_{SHEATH.sLEAFBASE}$	Promotion by i_{SHEATH} multiplied by $s_{LEAFBASE}$	8	-	-
$p_{sMARGINAL.sRIM}$	Promotion by $s_{MARGINAL}$ plus s_{RIM}	0.5	-	-
p_{sTIP}	Promotion by s_{TIP}	1	-	-
$t_{sLEAFBASE}$	Threshold of $s_{LEAFBASE}$	0.5	-	-
t_{sPROX2}	Threshold of s_{PROX2}	0.5	-	-
$t_{sPROX2B}$	Threshold of s_{PROX2}	0.9	-	-
t_{sRIM}	Threshold of s_{RIM}	0.8	-	-
t_{sTIP}	Threshold of s_{TIP}	0.3	-	-
K_{PER} Growth Phase 1				
$h_{CENTRAL.sTIP}$	Inhibition by $i_{CENTRAL}$ multiplied by s_{TIP}	-	-	1
h_{MID}	Inhibition by i_{MID}	1	1	1
$h_{PZMARGIN.MARGINAL}$	Inhibition by $i_{PZMARGIN}$ multiplied by $i_{MARGINAL}$	100	-	-
h_{sMID}	Inhibition by s_{MID}	1	-	-
h_{sMIDB}	Inhibition by s_{MID}	2	-	-
$h_{sMID.CENTRAL}$	Inhibition by s_{MID} multiplied by $i_{CENTRAL}$	-	1	1
$h_{sPZMARGIN}$	Inhibition by $s_{PZMARGIN}$	1	-	-
h_{sTIP}	Inhibition by s_{TIP}	5	5	5
m_{BLADE}	Multiplication of i_{BLADE}	0.5	0.5	0.5
$h_{sMARGINAL}$	Inhibition by $s_{MARGINAL}$	4	-	-
p_{DUL}	Promotion by i_{DUL}	-	-	1.5
$p_{sTIP.MID}$	Promotion by s_{TIP} multiplied by i_{MID}	-	-	2

p_{sRIM}	Promotion by s_{RIM}	25	6	6
t	Threshold of identity factor	-	-	0.1
t_{sRIM}	Threshold of s_{RIM}	0.8	0.7	0.7
t_{sTIP}	Threshold of s_{TIP}	-	-	0.5
K_{PER} Growth Phase 2				
$h_{LL.CENTRAL+LATERAL}$	Inhibition by i_{LL} multiplied by $i_{CENTRAL}$ plus $i_{LATERAL}$	-	-	100
$h_{PZMARGIN.MARGINAL}$	Inhibition by $i_{PZMARGIN}$ multiplied by $i_{MARGINAL}$	100	-	-
$h_{STBOUND}$	Inhibition by $i_{STBOUND}$	-	100	100
$h_{sMARGINAL}$	Inhibition by $s_{MARGINAL}$	1	-	-
$h_{sMID+MID}$	Inhibition by s_{MID} plus i_{MID}	1	-	1
$h_{sPZMARGIN}$	Inhibition by $s_{PZMARGIN}$	4	-	-
h_{sTIP}	First inhibition by s_{TIP}	4	-	-
m_{BLADE}	Multiplication of i_{BLADE}	0.5	0.5	0.5
$p_{DUL.sMID}$	Promotion by i_{DUL} multiplied by s_{MID}	-	-	5
$p_{STIPULE.sRIM.sSTBOUND}$	Promotion by $i_{STIPULE}$ multiplied by s_{RIM} and $s_{STBOUND}$	-	20	20
$p_{sMARGINAL}$	Promotion by $s_{MARGINAL}$	1.5	-	-
p_{sRIM}	Promotion by s_{RIM}	30	-	-
$t_{sLEAFBASE}$	Threshold of $s_{LEAFBASE}$	-	0.7	-
$t_{sMARGINAL}$	Threshold of $s_{MARGINAL}$	0.6	-	-
t_{sMID}	Threshold of s_{MID}	-	-	0.95
t_{sRIM}	Threshold of s_{RIM}	0.8	0.5	0.5
$t_{sSTBOUND}$	Threshold of $s_{STBOUND}$	-	0.7	0.7
t_{sTIP}	Threshold of s_{TIP}	0.2	-	-
K_{PER} Growth Phase 3				
$h_{MID+sMID+sTIP+PUL}$	Inhibition by i_{MID} plus s_{MID} plus s_{TIP} plus i_{PUL}	-	-	1
h_{sTIP}	Inhibition by s_{TIP}	1	3	-
m_{BLADE}	Multiplication of i_{BLADE}	3	-	-
m_{MID}	Multiplication of i_{MID}	-	-	10
m_{PUL}	Multiplication of i_{PUL}	-	-	2
m_{PZ}	Multiplication of i_{PZ}	0.5	0.5	0.5
m_{sMID}	Multiplication of s_{MID}	-	-	2
$p_{BLADE.sPROX2.sRIM}$	Promotion by i_{BLADE} multiplied by s_{PROX2} and s_{RIM}	2	-	-
$p_{BLADE.sPROX2.sTIP}$	Promotion by i_{BLADE} multiplied by s_{PROX2} and s_{TIP}	-	8	-
$p_{DUL.sMID}$	Promotion by i_{DUL} multiplied by s_{MID}	-	-	10
$p_{LEAFBASE}$	Promotion by $i_{LEAFBASE}$	-	1	-
$p_{OLATERAL}$	Promotion by $i_{OLATERAL}$	-	1	-
p_{sPROX2}	Promotion by s_{PROX2}	-	-	0.5
p_{sRIM}	Promotion by s_{RIM}	-	1	-
t_{sMID}	Threshold of s_{MID}	-	-	0.95
t_{sRIM}	Threshold of s_{RIM}	0.8	0.95	-

K_{PER} Growth Phase 4				
m_{PZ}	Multiplication of i_{PZ}	0.5	-	-
$m_{MARGINAL}$	Multiplication of $i_{MARGINAL}$	4	-	-
t_{sPROX2}	Threshold of s_{PROX2}	0.9	-	-
$t_{sPROX2B}$	Threshold of s_{PROX2}	0.5	-	-
t_{sRIM}	Threshold of s_{RIM}	0.8	-	-

Table S2. Parameters for the Tissue Sheet Models of Further Primordium Development (Fig.3, Fig.4)

Parameters relating to the model code in “Supplementary Text: Model Descriptions”, for all of the Tissue Sheet Models of Further Primordium Development. Parameters are denoted by m_x, p_x, h_x, or n_i, where X defines the factor the parameter relates to, m defines multiplication, p defines promotion and h defines inhibition, and n_i defines an additional general parameter. Each set of parameters are separated into those for K_{NOR}, K_{PD} and K_{PER} and then further subdivided into growth Phases 1-4. Model “WT Grass” refers to the Wildtype Grass Leaf Primordium model shown in Fig.3D-L and Fig.S4. “petiole-sheath” refers to the sheet model of the petiole-sheath hypothesis (Fig.4L-O,T-U, Fig.S5) and “Petiole-Leaf” refers to the petiole-leaf hypothesis (Fig.4P-S, Fig.S6).

Growth Phase	Maximum Resultant Areal Growth Rate					
	WT Grass	ns	Petiole-sheath	Petiole-sheath wox/prs1	Petiole-leaf	Petiole-leaf wox/prs1
Phase 1	11.3	11.1	12.5	12.3	31.4	31.4
Phase 2	13.7	13.7	17.6	18.5	12.2	6.4
Phase 3	25.2	22.3	26.7	15.7	13.8	5.0
Phase 4	17.5	19.4	-	-	-	-

Table S3. Maximum value of resultant areal growth rates for the 2D sheet models.

The maximum values of resultant areal growth rates for each phase of the models, shown in Fig. S7 (red values). Phase 1 stage is after timestep 0.7 when the petiole-sheath and petiole-leaf models diverge. The values are in arbitrary units and are given to allow comparisons between stages and models. They do not represent quantitative estimates of experimentally measured values. Model "WT Grass" refers to the Wildtype Grass Leaf Primordium model shown in Fig.3D-H and Fig.S7A. "*ns*" refers to the grass leaf model with the MARGINAL domain removed (Fig.3I-L, Fig.S7B). "Petiole-sheath" refers to the sheet model of the petiole-sheath hypothesis (Fig.4L-O, Fig.S7C). "Petiole-sheath *wox/prs1*" refers to the petiole-sheath model with the MARGINAL domain removed and the LATERAL domain truncated (Fig.4U, Fig.S7D). "Petiole-leaf" refers to the petiole-leaf hypothesis model (Fig.4P-S, Fig.S7E). "Petiole -leaf *wox/prs1*" refers to the petiole-sheath model with the MARGINAL domain removed and the LATERAL domain truncated (Fig.4V, Fig.S7F)

Growth Phase	Maximum Specified Growth Rates		
	WT Grass	Petiole-sheath	Petiole-leaf
Phase 1A	11.3	14.0	14.0
Phase 1B	11.3	14.0	16.5
Phase 2	12.6	12.1	8.6
Phase 3	20.7	20.9	6.0
Phase 4	19.8	-	-

1249 **Table S4. Maximum value of specified growth rates for the 2D models.**

1250 The maximum values of specified growth rates for each phase of the models, shown
1251 in Fig.S5-6 (dark orange regions). Phase 1B refers to Phase 1 before timestep 0.7
1252 and Phase 1B is after timestep 0.7. The values are in arbitrary units and are given to
1253 allow comparisons between stages and models. They do not represent quantitative
1254 estimates of experimentally measured values. Model “WT Grass” refers to the wildtype
1255 grass leaf primordium model (Fig.3 and Fig.S4). “Petiole-sheath” refers to the sheet
1256 model of the petiole-sheath hypothesis (Fig.4L-O, Fig.S5). “Petiole-leaf” refers to the
1257 petiole-leaf hypothesis model (Fig.4P-S, Fig.S6).

Movie S1. Volumetric models of primordium emergence: Formation of a ring primordium, Fig.2A-D, Fig.S2A-D

The model approximates a meristem apex with a dome-shaped volumetric canvas. The dome has a pre-pattern of abaxial (orange) and adaxial (blue) identities (Fig.2A-D). The primordial zone straddles the abaxial-adaxial midplane (green). Orthoplanar polarity points from the surface towards the midplane and axial (dark blue) domains. The specified growth rate is high perpendicular to orthoplanar polarity (Fig.S2A-D).

Movie S2. Volumetric models of primordium emergence: Formation of a sloping primordium, Fig.2E-F, Fig.S2E-F)

The model approximates a meristem apex with a dome-shaped volumetric canvas. The dome has a pre-pattern of abaxial (orange) and adaxial (blue) identities. The primordial zone straddles the abaxial-adaxial midplane (green) (Fig.3E-F). Orthoplanar polarity points from the surface towards the midplane and axial (dark blue) domains. The specified growth rate is high perpendicular to orthoplanar polarity, and is highest towards the midvein (Fig.S2E-F).

Movie S3. Volumetric models of primordium emergence: Formation of a grass leaf, Fig.2I-L,P-Q, Fig.S2G-H.

The wild-type grass leaf (Fig.2I-L) and *narrowsheath* mutant (Fig.2P-Q) models are shown. The models approximate a meristem apex with a dome-shaped volumetric canvas. Within the primordial zone (PZ) central (blue), lateral (red) and marginal (cyan) domains are defined. In the *narrowsheath* mutant model the marginal domain is removed, and the PZ truncated accordingly. Orthoplanar polarity points from the surface towards the midplane and axial domains. The proximal-distal polarity (PD) field points from the PZ boundary towards the midvein tip and meristem apex.

Specified growth rates are defined parallel to the orthoplanar field (K_{OP}), or PD field (K_{PD}), and perpendicular to both (K_{PER}). K_{OP} is low, K_{PD} is highest at the base in the central domain, and K_{PER} at the rim (Fig.S2G-H).

Movie S4. Volumetric models of primordium emergence: Formation of a eudicot leaf, Fig.4C-K

The wild-type eudicot leaf (Fig.4C-D), *prs* mutant (Fig.4E-F), *prs/wox1* mutant (Fig.4G-H), and ad-abaxial mutant (Fig.4I-K) models are shown. The models approximate a meristem apex with a dome-shaped volumetric canvas. Within the primordial zone (PZ) central (blue), lateral (red), outer lateral (dark red) and marginal (cyan) domains are defined. In the *prs* mutant model the marginal domain is removed, and the PZ truncated accordingly. In the *prs/wox1* mutant model the marginal and outer lateral domains are removed, and the PZ truncated accordingly. In the abaxialised mutant, adaxial identity is removed, leaving only abaxial identity (orange), the PZ is restricted to the central domain, and the midplane (green) is restricted to an axial domain. In all models, orthoplanar polarity points from the surface towards the midplane (green) and axial domains (dark blue) and the proximal-distal polarity (PD) field (blue arrows) points from the PZ boundary towards the midvein tip and meristem apex. Specified growth rates are defined parallel to the orthoplanar field (K_{OP}), or PD field (K_{PD}), and perpendicular to both (K_{PER}) (Fig. S2I-L).

Movie S5. Tissue sheet models of further primordium emergence: grass leaf development, Fig.3D-H,I-L, Fig.S4, Fig.S7A-B

The wild-type grass leaf (Fig.3D-H) and *narrowsheath* mutant (Fig.3I-L) models are shown. The models start with an initial ring with overlapping margins intersected by a clonal sector (yellow). The primordial zone (PZ) has central (blue), lateral (red) and

marginal (cyan) domains. In the *narrowsheath* mutant model the marginal domain is removed and the PZ accordingly truncated. At the end of phase 2 of the model, the proximal sheath domain (grey overlay) is introduced and further modulates growth rates. At timestep 0.7 the distal upper leaf (purple) and proximal upper leaf (orange), and lower leaf domains are indicated, but have no effect on growth rates. Specified growth rates parallel (K_{PD}) and perpendicular (K_{PER}) to PD polarity, and in thickness (K_{NOR}) are modulated by the different domains in the medial-lateral and proximal-distal axes (Fig.S4, Fig.S7A-B).

Movie S6. Tissue sheet models of further primordium emergence: Petiole-Sheath Hypothesis Eudicot Models, Fig.4L-O,T-U

The wild-type eudicot leaf (Fig.4L-O), *prs* mutant (Fig. 4T) and *prs/wox1* (Fig.4U) mutant models are shown. All three models start with an initial ring with overlapping margins. The primordial zone (PZ) is patterned in the mediolateral axis with central (blue), lateral (red), outer lateral (dark red) and marginal (cyan) domains. In the *prs* mutant model the marginal domain is removed and the PZ accordingly truncated. In the *prs/wox1* mutant model the marginal and outer lateral domains are removed, and the PZ accordingly truncated. At timestep 0.7 the distal upper leaf (purple) and proximal upper leaf (orange), and lower leaf domains are indicated, but have no effect on growth rates. At the end of phase 2 of the model, the proximal sheath domain (grey overlay) is introduced and further modulates growth rates. Specified growth rates parallel (K_{PD}) and perpendicular (K_{PER}) to PD polarity, and in thickness (K_{NOR}) are modulated by the different domains in the medial-lateral and proximal-distal axes.

Movie S7. Tissue sheet models of further primordium emergence: Petiole-Leaf Hypothesis Eudicot Models, Fig.4P-S,V, Fig.S6, Fig.S7E-F

The wild-type eudicot leaf (Fig.4P-S), and prs/wox1 (Fig.4V) mutant models are shown. Both models start with an initial ring with overlapping margins. The primordial zone (PZ) is patterned in the mediolateral axis with central (blue), lateral (red), outer lateral (dark red) and marginal (cyan) domains. In the prs/wox1 mutant model the marginal and outer lateral domains are removed, and the PZ accordingly truncated. At timestep 0.7 the distal upper leaf (purple), proximal upper leaf (orange), and lower leaf domains are introduced and used to modulate growth rates. At the end of phase 2 of the model, the proximal sheath domain (grey overlay) is introduced. Specified growth rates parallel (K_{PD}) and perpendicular (K_{PER}) to PD polarity, and in thickness (K_{NOR}) are modulated by the different domains in the medial-lateral and proximal-distal axes (Fig.S6, Fig.S7E-F).